Chapter 2. Nanocomposites photocatalysts for hydrogen production under visible light illumination

This chapter presents an introduction of heterogeneous photocatalysis. Different strategies to improve photocatalytic activity are discussed in detail. In addition, we discuss about the most visible-light active photocatalysts for hydrogen production and their structures are studied completely. We also review their recent development and heterojunction fabrications.

2.1 Fundamentals of heterogeneous photocatalysis

Reactions in chemical industries use catalysts that can be divided into two main group: homogeneous and heterogeneous catalysis. Homogeneous catalysis refers to reactions in which catalysts and reactants are in the same phase. However, heterogeneous catalysis is used where the phase of catalysts and reactants are different from each other. Phase includes solid, liquid and gas as well as immiscible liquids.[15]

Heterogeneous photocatalysis refers to a process where a semiconductor capable of absorbing photon energy of light is used as a catalyst. Generally, a photocatalytic reaction consists of three main steps: (I) a semiconductor absorbs light photons and generates excited electrons and holes; (II) these excited electrons and holes can migrate to the surface of semiconductor or recombine again inside the bulk material; (III) on the surface, holes can oxidize an oxidant (Equation.2.1) and electrons can reduce a reductant (Equation.2.2). Figure 2.1 illustrates schematically the main steps in heterogeneous photocatalysis reaction.

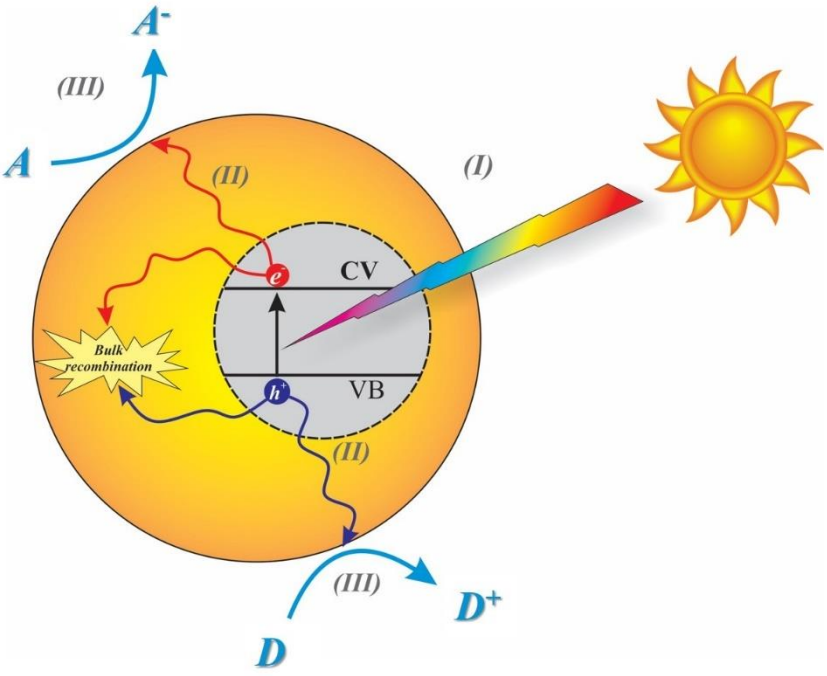

Figure 2.1. Schematic of heterogenous photocatalysis mechanism.

$$D + h^+ \rightarrow D^{\bullet+} \quad (2.1)$$

$$A + e^- \rightarrow A^{\bullet-} \quad (2.2)$$

If protons and oxygen in water are chosen to be reductant and oxidant, the process will become photocatalytic water splitting and half reactions of oxidation and reduction would be as follows:

$$H_2O + 2h^+ \rightarrow \frac{1}{2}O_2 + 2H^+ \quad (2.3)$$

$$2H^+ + 2e^- \rightarrow H_2 \quad (2.4)$$

Semiconductor band gap determines which wavelength of sunlight can be absorbed. The semiconductor with a wide band gap (E_{bg} > 3 eV) can only absorb UV light, which approximately accounts for 5% of solar energy (Figure 2.2).[16-18] In contrast, a narrow band gap semiconductor (E_{bg} < 3 eV) can be activated by visible light irradiation, which constitutes 43% of the sunlight spectrum.[19] Beside band gap, the positions of the valence and conduction bands are also very important in photocatalytic reactions. Figure 2.3 exhibited band structure, valence and conduction band positions of various semiconductors that can be used in various photocatalytic reactions.[20]

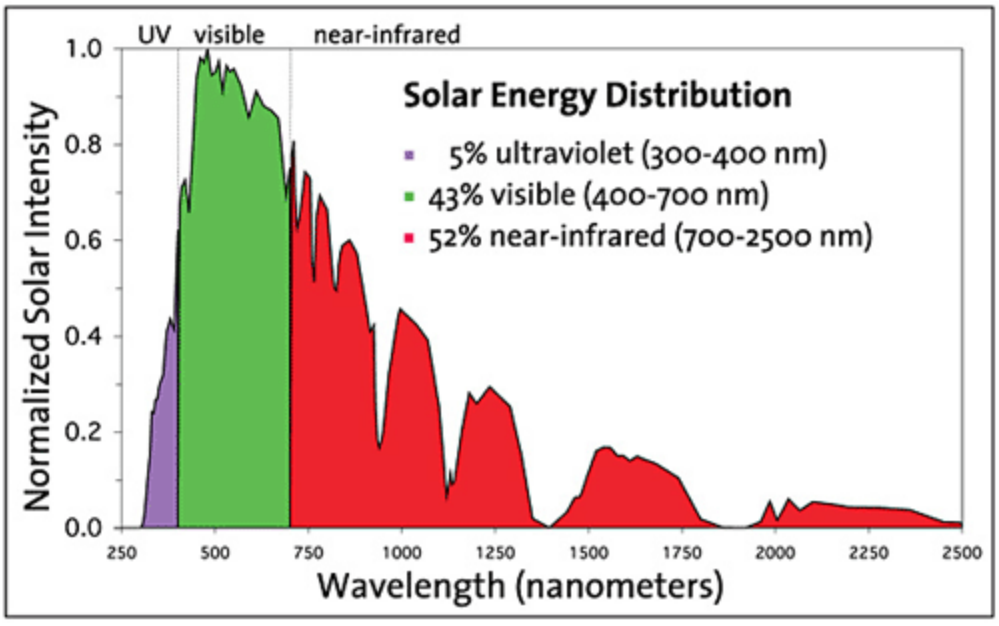

Figure 2.2. Solar energy distribution.[4]

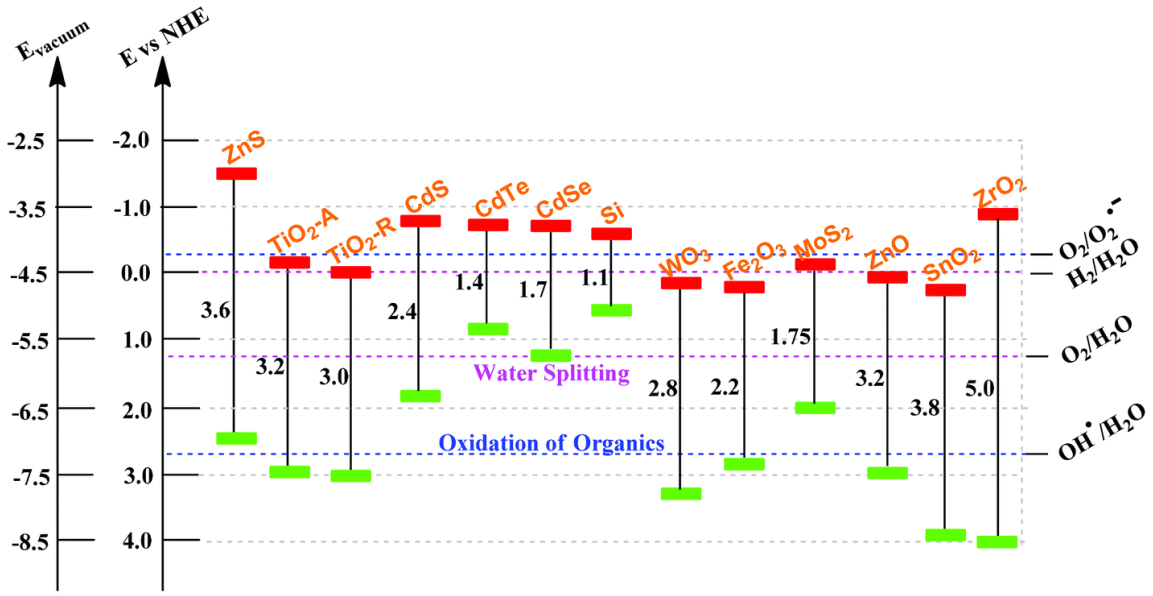

Figure 2.3. Band structure of various semiconductors.[20]

For H_2 evolution, the conduction-band edge should be more negative than the reduction potential of H^+ to H_2 ($E_{H^+/H_2} = 0\ V\ vs\ NHE\ at\ pH = 0$). On the other hand, the valence-band edge should be more positive than the oxidation potential of water ($E_{O_2/H_2O} = 1.23\ V\ vs\ NHE\ at\ pH = 0$) in order to evolve oxygen. Therefore, the band gap of semiconductor should be at least 1.23 eV in order to split the water. The equivalent light wavelength for this band gap energy is 1100 nm, which is in near-infrared region of the sunlight spectrum. By considering other factors such as energy losses during different stages in the photocatalytic process, effective semiconductors should have band gaps larger than 2 eV, which is related to the light with wavelength lower than 620 nm.[21, 22] Although some semiconductors can absorb the infrared light by photon up-conversion mechanism, their applications are usually limited to degradation of organic compounds.[23-26]

2.1.1 Overall water splitting

Fujishima and Honda were pioneers in decomposing water with light illumination.[6] They discovered that TiO_2 and Pt can act as anode and cathode electrodes, respectively, in a

photoelectrochemical cell. This system could split water into hydrogen and oxygen under intense UV irradiation. Some years later, Bard applied the concept of this system to introduce photocatalysis process.[8] Since then, there have been enormous efforts on developing semiconductors that can decompose water into H_2 and O_2 under the light illumination.

To decompose water directly into hydrogen and oxygen under sunlight irradiation is the ultimate goal of photocatalytic hydrogen generation system. In this process, a semiconductor with proper band-edges can absorb photon energy and evolve hydrogen and oxygen simultaneously. However, this reaction is thermodynamically non-spontaneous with the Gibbs free energy of 237 kJ/mol.[27]

$$2H_2O \xrightarrow{photon\ energy} 2H_2 + O_2 \qquad (2.5)$$

Some semiconductors can absorb UV light and split water directly into hydrogen and oxygen, but most of them have an energy conversion efficiency less than 1%.[28-30] Moreover, they cannot produce hydrogen and oxygen in a stoichiometric ratio because one type of charge carriers is accumulated on the surface of photocatalyst.[27] One exceptional example is a GaN-ZnO solid solution photocatalyst that can split water into hydrogen and oxygen stoichiometrically under visible light illumination with a quantum efficiency of about 6%.[31] It is obvious that overall water splitting is very difficult to be proceeded under visible light illumination and becomes one of the greatest challenges for researchers in this field.

2.1.2 Sacrificial reagent systems

It is believed that the overall water splitting is a very hard reaction to be proceeded, and it needs a specific kind of semiconductor with appropriate band edge positions. Nevertheless, some semiconductors can do one of the half reactions of water splitting, i.e. water reduction or oxidation, in the presence of suitable sacrificial reagents (electron donors or acceptors). In principle, sacrificial agents usually react with one type of charge carriers while the other carrier reacts with water to produce hydrogen or oxygen. Electron donors, which consume excited holes on the surface of the semiconductor, are used for water reduction half reaction and electron acceptors (electron scavengers) are usually needed for water oxidation, as illustrated in Figure 2.4. Generally, the

electron donors must be more readily oxidized than water by excited holes, while the electron acceptors must be more readily reduced than water by excited electrons. The most common electron donors are methanol, ethanol, triethanolamine (TEA) and an aqueous solution of Na_2S/Na_2SO_3, whereas metal cations such as Ag^+ and Fe^{3+} are usually utilized as electron acceptors.[27]

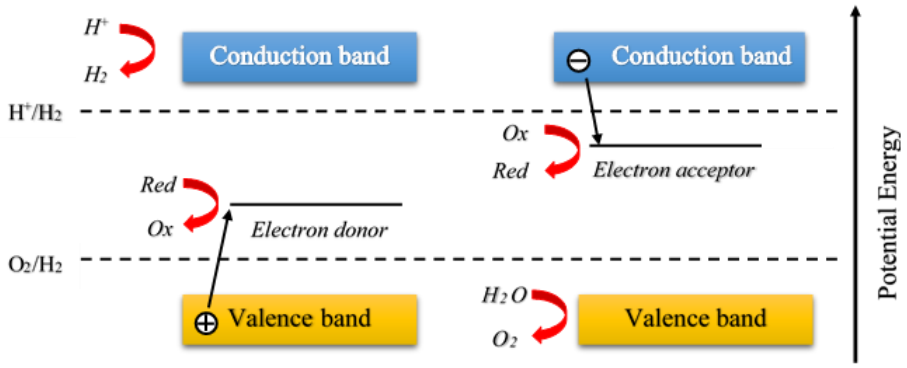

Figure 2.4. Schematic principles of water reduction or oxidation in the presence of sacrificial reagents.[27]

Various mechanisms were proposed to explain the consumption of sacrificial reagents in hydrogen production reactions.[30, 32] These electron donors react more easily with holes than water due to its less positive oxidation potential. This would lead to accelerated holes consumption on the surface of the photocatalyst and so the positive charge accumulation is partially prevented and, as a result, protons and photoexcited electrons can react together more easily. It should be noted that, in the case of using methanol as electron donor, hydrogen is also produced as a result of methanol conversion (Equation.2.6).[33, 34] However, by increasing the carbon chain length, the contribution of H_2 production from alcohol conversions decrease substantially.[34] Moreover, Guzman showed that the direct reaction of methanol with excited holes does not proceed to an appreciable extent in the presence of high concentration of water.[35]

$$CH_3OH + H_2O \rightarrow CO_2 + 3H_2 \qquad (2.6)$$

Semiconductors capable of decomposing water in the presence of sacrificial agents may seem to be useless. Nevertheless, these photocatalysts not only can be used in Z-schematic system but also some of them can be used to produce H_2 using biomass derived sacrificial reagents.[36, 37]

2.1.3 Electron mediator systems

The electron mediator system is also called Z-scheme system or a dual photocatalyst system. The concept of this system is to transfer charge carriers by two different electron mediators in a solution and after participating in redox reactions, they all return to their original chemical states.[38] This procedure for overall water splitting is entirely different than two previous methods. It needs two various photocatalysts: a semiconductor provides photoexcited electrons to participate in half-reaction for H_2 evolution; another one supplies photogenerated holes to take part in half-reaction of water oxidation. Moreover, the two semiconductors should be excited simultaneously and one half of charge carrier will recombine in order to bring electron mediator in their original states (Figure 2.5). Some of the most common electron mediators are Fe^{3+}/Fe^{2+}, IO^{3-}/I^{-} and Ce^{4+}/Ce^{3+}.[39]

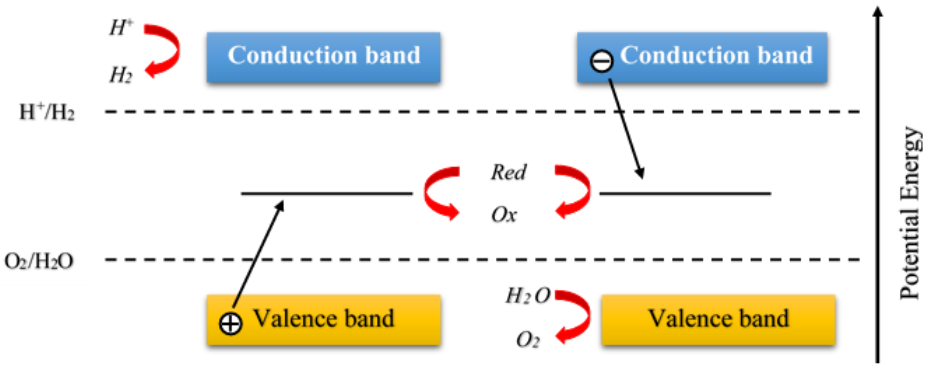

Figure 2.5. Schematic principles of overall water splitting in the Z-scheme system.[38]

There are some review papers discussing different approaches and application of this dual step system, which is similar to plant photosynthesis.[38, 40] Nonetheless, this system has some drawbacks in comparison with the one-step system. For instance, Z-scheme systems are usually more complicated and need more photons to produce the same amount of hydrogen because half of the excited charges are used in order to bring the excited mediator to its ground state for further reactions.[38, 41]

2.1.4 Activity and quantum efficiency

Photocatalytic activity depends on many factors such as light source (Xe or Hg lamps), light intensity, reaction cell, different directions of irradiation (top, inner, or side), reaction media (water or various sacrificial agents), and the quantity of photocatalyst. The simplest way to find semiconductor activity is to measure the amount of evolved gases in a specific period of time and report it in $\mu mol \cdot h^{-1}$ or $\mu mol \cdot h^{-1} \cdot g^{-1}$ units.[39]

Quantum yield (Quantum efficiency) is another way to report photocatalytic activity of a semiconductor. This is independent of effective factors that are mentioned above and it is defined as:[42]

$$Quantum\ yield\ (\%) = \frac{Number\ of\ reacted\ electrons}{Number\ of\ absorbed\ photons} \times 100 \qquad (2.7)$$

Despite this equation can give us accurate quantum yield, it is very hard to measure the real amount of absorbed photons. In order to solve this problem, researchers suggested to use apparent quantum yield, which is declared as follows:[39]

$$\begin{aligned} &Apparent\ quantum\ yield\ (\%) \\ &= \frac{Number\ of\ reacted\ electrons}{Number\ of\ incident\ photons} \times 100\% \\ &= \frac{2\ \times\ Number\ of\ evolved\ H2\ molecules}{Number\ of\ incident\ photons} \\ &\times 100\% \\ &= \frac{4\ \times\ Number\ of\ evolved\ O2\ molecules}{Number\ of\ incident\ photons} \\ &\times 100 \end{aligned} \qquad (2.8)$$

It is obvious that the apparent quantum yield is smaller than the real quantum efficiency because of the difference between the number of absorbed photons and incident light.

Solar energy conversion efficiency is a method to calculate solar cell efficiency, it can also be used to report the photocatalytic activity of a semiconductor.

$$Solar\ energy\ conversion\ efficiency\ (\%) = \frac{Output\ energy\ of\ H2\ evolved}{Energy\ of\ incident\ solar\ light} \times 100\% \quad (2.9)$$

Up to now, semiconductors have extremely low solar energy conversion values and so this indicator is seldom used.[28] It is anticipated that for industrial application of water splitting via sunlight, this efficiency should improve noticeably.

2.1.5 Cocatalysts

A cocatalyst is a compound added to the semiconductors photocatalyst to improve their activity. In photocatalytic water splitting, the cocatalysts can be used to enhance either the water oxidation or reduction reactions. The cocatalyst for water reduction are usually small metal nanoparticles which can form Schottky junction with semiconductors and enhance charge separation in photocatalyst or photoelectrochemical cell.[43, 44] In principle, the contact between metal and semiconductor creates an electric field that separate excited electrons and holes more easily, as demonstrated in Figure 2.6.[45-47] If the work function of the metal matches the conduction band-edge of semiconductor, excited electrons move from the semiconductor to the metal and from there, they can react with water. In addition, the metal provides active sites for hydrogen generation due to its relatively low over-potential for water reduction.

The physical and chemical properties of cocatalyst such as particle size and valence states, which significantly affect their performance, are strongly dependent on the cocatalyst loading methods. Although depositing more cocatalysts provide more active sites for reactions, they reduce the absorption ability of the photocatalyst. Therefore, the concentration of cocatalysts should be optimized to obtain the maximum activity during water splitting under light illumination.

There are two main techniques to deposit cocatalysts on the surface of semiconductors: in situ photodeposition and impregnation. In the first one, cocatalyst is reduced by photoexcited electrons on the surface of a semiconductor under light irradiation in the presence of sacrificial reagents. Therefore, the semiconductor should be mixed with a precursor solution of cocatalyst. If

photo-reduction step is performed with various precursors, a core-shell structure can be achieved easily.[48]

The second one is usually followed by a post-calcination step. First, a semiconductor is impregnated with a solution containing the cocatalyst precursor and then evaporated and dried. After this stage, the dry mixture is calcined in air or other gases such as hydrogen or argon in order to obtain desired states of metal or metal oxide. The final state of cocatalyst depends on gas treatment, temperature and type of precursor.[39]

There have been great efforts to use different types of cocatalysts including transition metals, metal oxides and noble metals for each half reaction of water splitting. The most common cocatalysts for hydrogen evolution are Pt, Rh, Au, NiO and RuO_2. [49-51] [52] [53] [54] Other types such as the core shell configuration of cocatalysts have been recently proposed to improve H_2 evolution in overall water splitting.[48, 55]

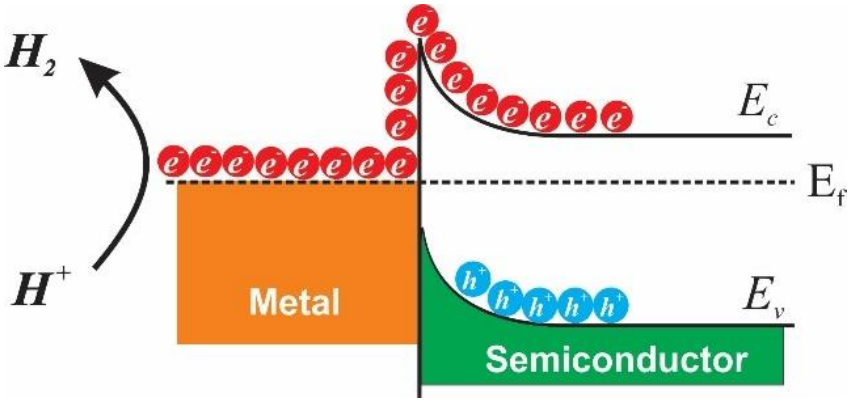

Figure 2.6. A schematic energy band model of Schottky junction.[45-47]

2.1.6 Semiconductor heterojunction structures

Instead of using a single semiconductor, combining a semiconductor with other semiconductors, metals, and molecules would lead to form a heterojunction structure between them. These heterojunctions were found to enhance the performance of various devices such as solar cells, photoluminescence and electro-chromic devices.[13, 56, 57] In addition, the utilization of nanocomposites as photocatalyst instead of a single semiconductor, is another efficient and practicable approach to enhance the photocatalytic performance. In this kind of nanocomposite, excited charges migrate from one semiconductor to another semiconductor (or metal which acts as

a cocatalyst). The second semiconductor should have proper band-edge position or higher efficiency in comparison with the first one. Furthermore, this nanocomposite can improve its efficiency due to the fact that reduction and oxidation reactions happen on two different components.[58]

All of heterojunctions can be categorized into three types based on their conduction and valence band positions, as illustrated in Figure 2.7. In Type 1, both excited electrons and holes move from semiconductor 1 to semiconductor 2 due to their band edge positions. Usually this kind of heterojunction doesn't improve photocatalysts because of accumulation of both charge carriers on one semiconductor.

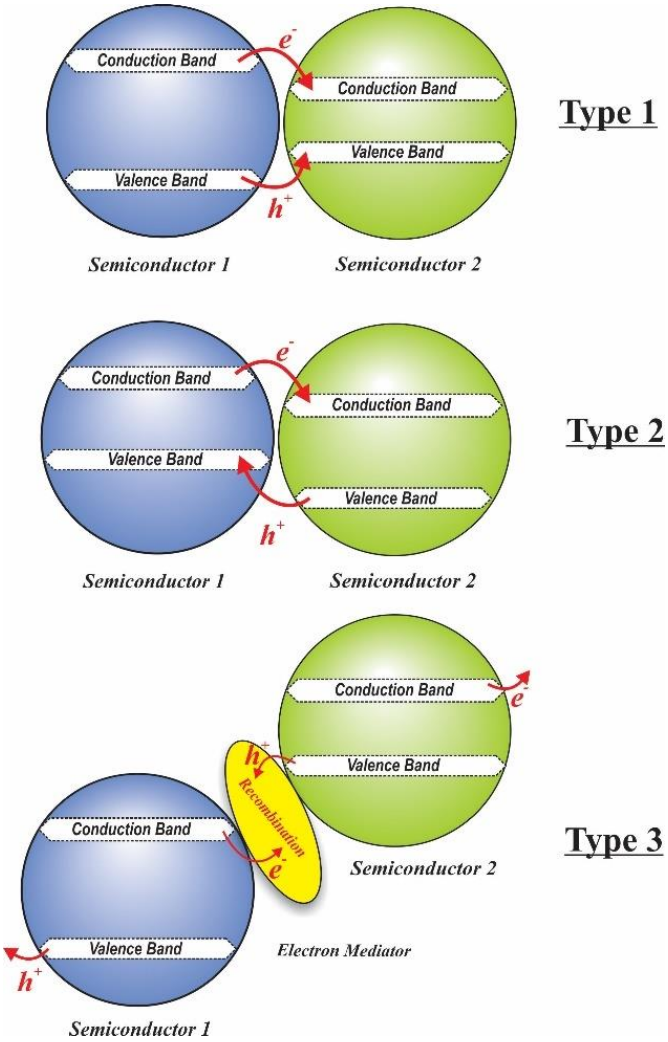

Figure 2.7. Various kinds of heterojunctions.[58]

In the second group of heterojunctions, the conduction band of semiconductor 2 is lower than that of semiconductor 1. However, the valence band of semiconductor 1 has higher value than that of semiconductor 2. As a result, excited electrons can move from semiconductor 1 to 12, although generated holes migrate vice versa. If both semiconductors have sufficient intimate contacts, an efficient charge separation will occur during light illumination. Consequently, charge recombination is decreased and charge carriers have longer lifetime, which results in higher photocatalyst activity. Most of the composites discussed in the literature, are of type 2.

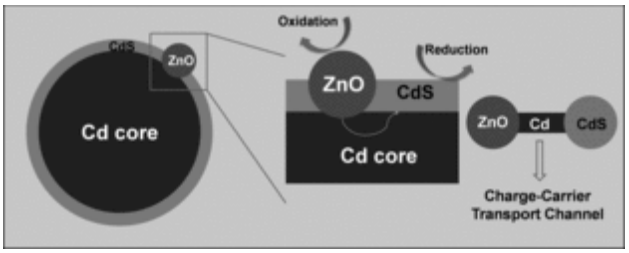

Figure 2.8. Scheme of the improving mechanism of photoexcited charge-carrier transport in the ZnO–CdS@Cd heterostructure.[59]

Type 3 consists of semiconductors with both valence and conduction bands being lower in one than the other, as can be seen from Figure 2.7. This kind can be applied in the Z-scheme system with an appropriate electron mediator or some kind of bridges that attach the two semiconductors. For instance, Wang et al. synthesized a core-shell nanocomposite of ZnO–CdS@Cd in such a way that Cd element acts as the charge-carrier bridge.[59] A schematic of this nanocomposite is demonstrated in Figure 2.8.

2.2 Titanium dioxide photocatalysts

In nature, Titanium dioxide (TiO_2) has three crystal phases including: anatase (tetragonal), rutile (tetragonal), an brookite(orthorhombic).[60-62] Various forms of TiO_2 have slightly different band gaps of around 3 eV (anatase: 3.2 eV, rutile: 3 eV), due to the variety of the crystal structures as demonstrated in Figure 2.9.[63, 64] Both anatase and rutile have the same construction unit of TiO_6, although the distortion of their crystal structure gives them different photocatalytic activities. Rutile is the thermodynamically stable form, and brookite does not usually show appreciable photocatalytic activity, but anatase is often indicated as the most active phase.[65, 66] The redox

potential of TiO_2 valence band is +2.53 V (vs. NHE at pH=0), that can evolve oxygen from water. Moreover, its redox potential of photoexcited electrons is -0.52 V(vs. NHE at pH=0), which is negative enough to produce hydrogen from water.[67, 68]

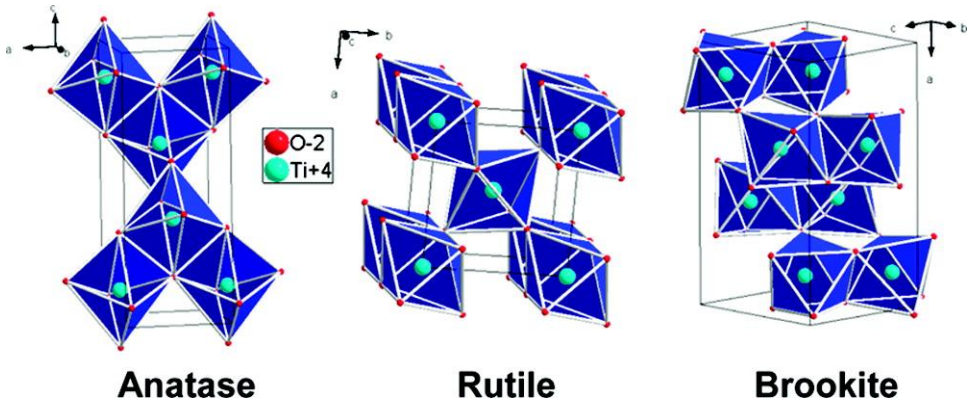

Figure 2.9. Representations of the TiO2 anatase, rutile, and brookite forms.[62]

TiO_2 possesses specific properties that make it almost a perfect photocatalyst for hydrogen production via sunlight energy. These features are: activity in catalyze photocatalytic reaction, ability to activate under sunlight energy, chemically inert and stable under photocatalytic reaction, large specific surface area and low cost. However, its large band gap (> 3 eV) limits its application in visible light region that accounts for a large amount of solar energy. Thus, various methods such as doping with anions and cations have been suggested to decrease its band gap and harvest more visible light energy.[66-70] Moreover, some researchers tried to improve TiO_2 kinetic efficiency by controlling the particle size or increasing its surface area in order to generate more hydrogen under sunlight illumination.[70-73]

After absorbing photon energy, a semiconductor produces excited electrons and holes. The charge carriers are separated or recombined together during their path to the surface of the semiconductor. Clearly, this step plays an important role in determining the light to fuel conversion efficiency.[74] Thus, many efforts has been made to synthesize various junction approach in order to enhance charge separation process. They can be categorized in two main groups as follows: heterojunction with other narrow band gap semiconductors, various phase junction of TiO_2.

2.2.1 Heterojunction of TiO_2 and other semiconductors

Based on discussion in semiconductor heterojunction structures, Type 2 configuration (Figure 2.7) is the best way to increase hydrogen production from TiO_2 and other semiconductors.[75, 76] This structure helps to increase charge separation and enhances carrier's lifetime. Therefore, excited electrons and holes have more time to react with adsorbed radicals on the active sites and as a result, hydrogen production increases significantly compared with pristine semiconductors.

TiO_2 and CdS were the most studied semiconductors during the last decades due to their photocatalytic properties and benefits.[74, 77] However, each of them has some drawbacks that limit their application for hydrogen production from sunlight. For example, TiO_2 has a wide band gap inapplicable for visible light absorption and CdS is instable during photocatalytic reactions. The combination of these semiconductors in nanoscale leads to have more efficient photocatalysts that can generate hydrogen under visible light irradiation with high stability. Under visible light illumination, CdS can absorb photons and produce holes and electrons. Although TiO_2 cannot absorb visible light, due to its wide band gap, excited electrons can move from CdS to TiO_2. This leads to a better charge separation, and results in higher quantum yield. It should be noted that the excited holes remain in the valence band of CdS and from there; they can oxidize any sacrificial agents. [78, 79] Various nanocomposites with different morphologies can be created CdS and TiO_2, which can be generally classified into two groups: CdS nanoparticles on the surface of TiO_2 or TiO_2 nanoparticles deposited on the surface of CdS. Some important morphologies will be discussed here, which resuls in higher light absorption and higher hydrogen evolution in the visible light region.

Generally, two different morphologies for mixing CdS nanoparticles and titanate nanotubes have been proposed in order to improve photocatalytic activity, as illustrated in Figure 2.10.[80-84] CdS/titanate nanotubes (CdS/TNTs) were reported to have higher increase in photocatalytic activity in comparison with traditional nanocomposite CdS@TNTs.[80] The CdS/TNTs nanostructures lead to have a proper dispersion of CdS as well as intimate multipoint contacts between two nanocrystals. It is clear that the ratio of Cd/Ti plays an important role in photocatalyst activity. The optimum value of this proportion was 0.05, which corresponds to 6 wt% of CdS in photocatalysts. With the optimum cocatalyst quantity of Pt (2.0 wt%), the CdS/TNTs could

generate 353.4 μmol h^{-1} hydrogen with 25.5% quantum yield under visible light. Nevertheless, the quantum yield of traditional CdS@TNTs could hardly reach 2.7% and as mentioned before, changing the structure of nanoparticles can have major impacts on their activity. It is noteworthy that this nanocomposite was stable for hydrogen production during 120 h of 6 cycles. Therefore, this nanostructure improved noticeably the stability of photocatalyst during hydrogen evolution.

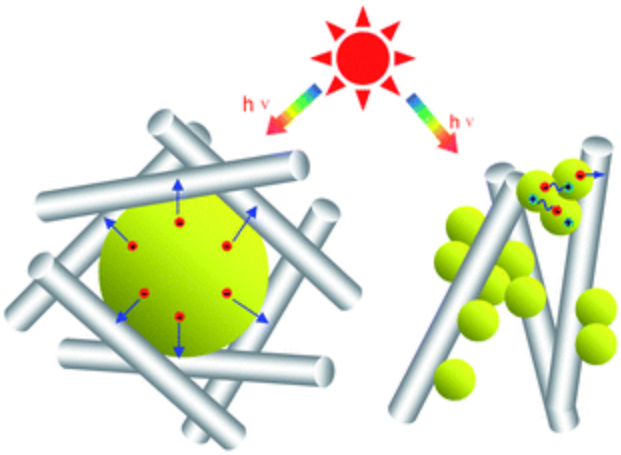

Figure 2.10. Schematic illustration of the two different architectures in CdS/TNTs (left) and CdS@TNTs (right).[80]

Many researchers have investigated the deposition of CdS nanoparticles inside different nanostructure of titanate such as tubular and nanotubes with the aim of obtaining highly efficient nanocomposites.[81, 85] Li et al. deposited homogeneously CdS nanoparticles inside the TiO_2 nanotubes.[81] They examined its photocatalytic water splitting with electron donors containing S^{2-}, SO_3^{2-} at wavelength of 420 nm. They attained 43.4% quantum yield for H_2 evolution. This is due to the quantum size effect of CdS nanoparticles as well as synergetic effects between two nanocomposites. This also means that the potential energy at the interface of CdS and TiO_2 would help electrons to transfer from CdS to TiO2 more easily and consequently enhance photocatalytic activity.

CdS nanoparticles can also be deposited on nanosheets of titanate that leads to increase quantum yield of nanocomposite.[85-88] The powerful interaction between titanate 2D nanostructures and CdS helped to create visible light absorption photocatalysts with high stability towards photocorrosion of CdS. Our group synthesized an ultrathin titanate nanodisks (TNDs) by the solvothermal method.[89] After that, we deposited both CdS nanoparticles as a visible light

semiconductor and Ni nanoparticles as a cocatalyst on the surface of TNDs for hydrogen evolution. This nanocomposite was able to separate photoexcited charges efficiently and as a result it showed a very high activity for water splitting under visible light irradiation. The concept of depositing cocatalysts on the other surface (here on TNDs), would help to enhance photocatalytic activity by increasing charge separation and preventing recombination phenomena. As can be seen in Figure 2.11(a), excited electron can easily transfer from CdS to TNDs and from there to Ni cocatalyst [86]. With an optimum ratio of CdS/TNDs and Ni loading, this nanocomposite can generate H_2 from water-methanol solution under visible light irradiation. The hydrogen evolution rate was 15.326 mmol g^{-1} h^{-1} during 15 h of reaction, which results in having 24% quantum yield at $\lambda \geq$ 420 nm. It is noteworthy that this approach of mixing semiconductors with TND can also be used for other efficient visible light active semiconductor. The intimate contact between TND and CdS plays a crucial role in this kind of nanostructure. In other words, physical mixing of this semiconductors cannot result in high photocatalyst activity. By growing CdS and Ni nanoparticles on the surface of TND by means of ion exchange method we were certain that nanoparticles had intimate contact and so charge carriers can easily transfer between semiconductors, as shown in Figure 2.11(b).[90]

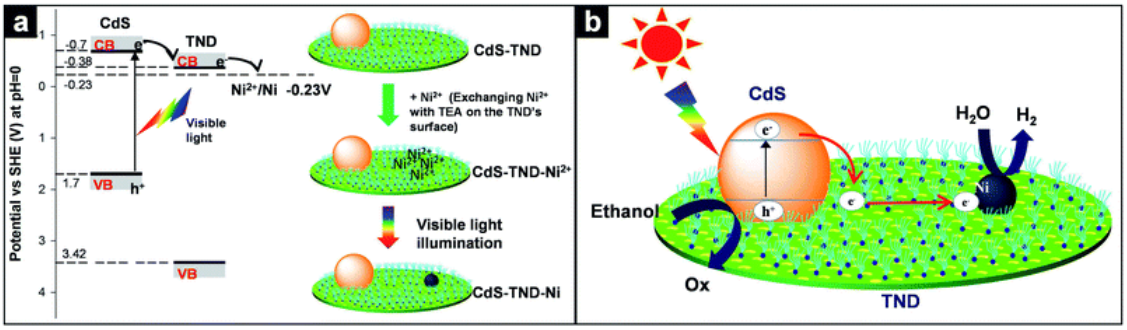

Figure 2.11. Schematic illustration of the electron transfer in the photoreduction of Ni^{2+} adsorbed on the surface of TNDs under visible light illumination and schematic illustration of the formation of Ni clusters on the surface of TND by visible-TND composites by visible light illumination (a). Schematic illustration of the charge transfer in CdS-TND-Ni MPs in the photocatalytic H_2 production from water-ethanol solution under visible light (b).[86]

In another technique, researchers tried to deposit TiO_2 nanoparticles on CdS nanostructures.[78, 79, 91-93] In most of them, a cocatalyst should be utilized in order to have hydrogen production. For instance, Jang et al. made a nanocomposite of CdS nanowires with a high crystallinity, which had TiO_2 nanocrystals on their surfaces, as shown in Figure 2.12.[79] Under

visible light, this nanostructure displayed hydrogen production from an aqueous solution of sulfide and sulfite ions. The optimum ratio of TiO_2 in this nanostructure would be 0.2, which led to having the highest activity under visible light irradiation. The possible role of TiO_2 NP is to provide sites for collecting the photoelectrons generated from CdS NW, enabling thereby an efficient electron-hole separation as depicted in Figure 2.12.

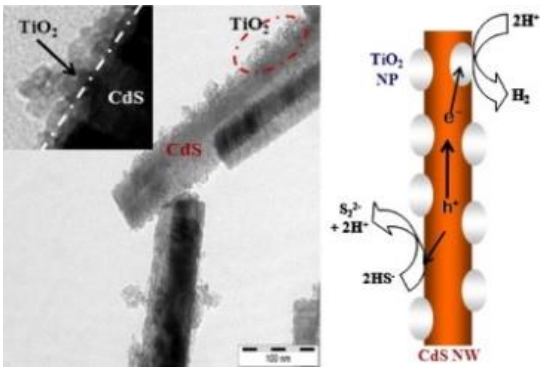

Figure 2.12. A nanocomposite consisting of CdS NW with high crystallinity decorated with nanosized TiO_2 NPs.[79]

Preparing nanocomposite is a very delicate process and each step should be considered precisely, even though the nanostructure and crystallinity may change with the order of adding precursors. Park et al. showed that reversing chemical precipitation order of CdS on TiO_2 nanoparticles caused to have different H_2 evolution rates in H_2 evolution under the same conditions.[94] They prepared CdS_R by adding Cd^{2+} in aqueous solution containing S^{2-} and Pt-loaded TiO_2. Another nanocomposite with an equal molar ratio was prepared by adding sulfide drops into the solution of Cd^{2+} and Pt-TiO_2 (Cd_RS). Surprisingly, CdS_R showed 10 times higher hydrogen evolution than Cd_RS under visible light irradiation (Figure 2.13).

Khatamian et al. prepared a metalosilicate-based (ferrisilicate and aluminosilicate) nanocomposite of CdS/TiO_2 via hydrothermal method.[95] Utilizing metalosilicate support has many advantages such as offering high surface area and providing homogenous dispersion of CdS nanoparticles. Moreover, this support both prevents agglomeration of the semiconductor and facilitates electron transfer and separation. It is noteworthy to consider that applying ferrisilicate, the presence of partially occupied d orbitals of Fe^{3+}, which can interact with TiO_2 orbitals, enhances the photocatalytic activity, while applying aluminosilicate as a support didn't improve its activity

compared to unsupported composite. In the case of CdS phase, hexagonal structure showed around sixfold higher photocatalytic activity than cubic one.

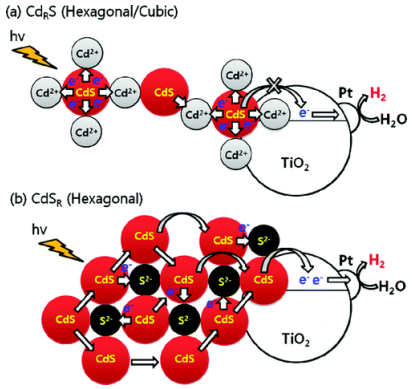

Figure 2.13. Schematic illustration for photocatalytic hydrogen production mechanisms of Cd_RS and CdS_R hybrids.[94]

Vu et al. provided nanocomposite of TiO_2 nanorods and CdS nanoparticles with Ni clusters in order to enhance charge separation and photocatalytic activity.[84] A dominant feature of this nanorod-based materials is that nanoparticles of the second semiconductor could be dispersed uniformly on the nanorod surface. Ni nanoparticles acting as cocatalysts were deposited on the surfaces of these nanorods selectively. This configuration can improve the efficiency of electron transfer from the sensitized CdS nanoparticles to TiO_2 and then to Ni clusters, as depicted in Figure 2.14. The H_2 production rate was 33.36 μmol h^{-1} g^{-1} under visible light in the presence of methanol as a sacrificial reagent, which was about 44 times higher than neat Ni-CdS system. Table 2.1 summarized different nanocomposites of CdS and TiO_2 with their hydrogen production and quantum yields.

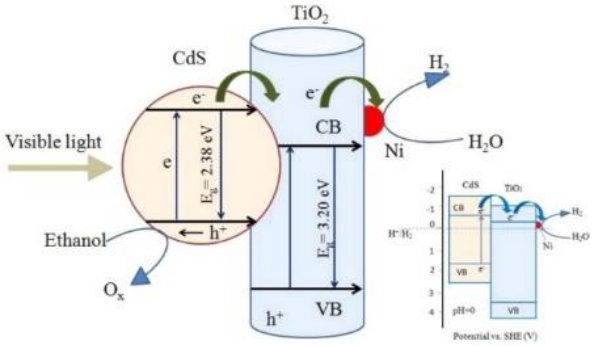

Figure 2.14. Mechanism illustration of the activity of Ni–TiO_2/CdS under visible light for the production of H_2; inset is the potential redox energy corresponding to CdS, TiO_2, and H^+/H_2.[84]

Table 2.1. Different nanocomposites of CdS and TiO2.

Semiconductor 1	Semiconductor 2	Cocatalyst	Sacrificial reagent	Light Source	Hydrogen production ($\mu mol\ h^{-1}\ g^{-1}$)	Quantum yield (%)	Refs
$Na_2Ti_2O_4(OH)_2$ nanotube	CdS	Pt	Na_2S/Na_2SO_3	350 W Xe, $\lambda \geq 430nm$	545	2.7 at λ = 430 nm	[83]
TiO_2 nanotubes	CdS	Pt	Na_2S/Na_2SO_3	300 W Xe, $\lambda \geq 420nm$	2680	43.3 at λ = 420 nm	[81]
Titanate nanotubes	CdS	Pt	Na_2S/Na_2SO_3	500 W Xe, $\lambda \geq 430nm$	1767	25.5 at λ = 420 nm	[80]
Titanate nanodisks	CdS	Ni	Ethanol	300 W Xe, $\lambda \geq 420nm$	11038	21 at λ = 420 nm	[89]
Titanate nanodisks	CdS	Ni	Ethanol	300 W Xe, $\lambda \geq 420nm$	15326	24 at λ = 420 nm	[86]
TiO_2 nanosheet	CdS nanoparticles	---	Na_2S/Na_2SO_3	350 W Xe, $\lambda \geq 400nm$	1651	8.9 at λ = 420 nm	[96]
TiO_2	CdS	Pt	Na_2S/Na_2SO_3	450 W Xe, $\lambda \geq 420nm$	4848	No data	[94]
TiO_2	Hexagonal CdS	---	Na_2S/Na_2SO_3	500 W Osram	8990	No data	[95]
TiO_2 nanorods	CdS nanoparticles	Ni	Ethanol	300 W Xe, $\lambda \geq 420nm$	33.63	No data	[84]
Titanate nanotubes	$Cd_{0.5}Zn_{0.5}S$	---	Na_2S/Na_2SO_3	500 W Xe, $\lambda \geq 430nm$	1738.5	38.1 at λ = 420 nm	[97]
TiO_2 nanosheet	CdS NPs	Pt	Lactic acid	350 W Xe, $\lambda \geq 420nm$	6625	13.9 at λ = 420 nm	[87]
TiO_2	CdS	Pt	Na_2S/Na_2SO_3	350 W Xe, $\lambda \geq 420nm$	6720	4.5 at λ = 420 nm	[98]
Titanate spheres	CdS nanoparticles	---	Na_2S/Na_2SO_3	300 W Xe, $\lambda \geq 420nm$	75	No data	[99]

Table 2.1 Continue.

Semiconductor 1	Semiconductor 2	Cocatalyst	Sacrificial reagent	Light Source	Hydrogen production ($\mu mol\ h^{-1}\ g^{-1}$)	Quantum yield (%)	Refs
nanometer-thick layered titanate nanosheet	CdS quantum dots (QDs)	---	Na_2S/Na_2SO_3	300 W Xe, $\lambda \geq 420nm$	1000	No data	[100]
Bulk CdS	TiO_2 nanoparticles	Pt	Na_2S/Na_2SO_3	350 W Xe, $\lambda \geq 420$ nm	6400	No data	[78]
hex-CdS	TiO_2	Pt	glycerol	300 W Xe, $\lambda \geq 420$ nm	22	No data	[93]
TiO_2	CdS				65		
CdS nanowires	TiO_2 nanoparticles	Pt	Na_2S/Na_2SO_3	500 W Xe, $\lambda \geq 420$ nm	110	No data	[79]
CdS bulk	TiO_2 nanoparticles	Pt	Na_2S/Na_2SO_3	350 W Xe, $\lambda \geq 420$ nm	4224	No data	[91]
Chromosilicate	CdS–TiO_2	---	Na_2S/Na_2SO_3	500 W Osram, , $\lambda \geq 420$ nm	2580	76.27at λ = 450 nm	[101]
TiO_2	CdS	Au	Na_2S/Na_2SO_3	300 W Xe, $\lambda \geq 420$ nm	1970	No data	[92]

Some researchers synthesized nanocomposites of TiO_2 and some of the metal oxides which are activated in the visible light region.[102-110] Interestingly, some of them showed higher hydrogen production in comparison with pristine TiO_2 due to visible light absorption and better charge separation. For instance, Martha et al. tried to increase hydrogen production by combining doped TiO_2 with V_2O_5.[105] Although N, S doped TiO_2 has a very low hydrogen evolution, the combination of the doped-TiO_2 with V_2O_5 exhibited 7 times higher hydrogen production under visible light irradiation (296.6 $\mu mol\ h^{-1}$). Xie et al. showed that nanocomposite of $TiO_2/BiVO_4$ had a much longer lifetime of photoexcited charge carriers and so higher charge separation.[109] The main reason for this phenomenon is related to high movements of photoexcited electrons from

$BiVO_4$ to TiO_2. Due to this reason, this photocatalyst had unexpected visible light activity for water splitting rather than $BiVO_4$ which was almost inactive in this region. They reported that $TiO_2/BiVO_4$ with molar ratio of 5%, could evolve 2.2 mol h^{-1} hydrogen, which was much higher than mixing with reduced graphene oxide nanosheet (0.75 mol h^{-1}) under the similar conditions.[110] Another group deposited Fe-TiO_2 nanoparticles (FTO) on the surface of $CaIn_2O_4$ nanorods (CIO).[107] This nanocomposite revealed hydrogen production in the presence of KI as sacrificial agent and Pt as cocatalyst. The contact of these two nanoparticles facilitated charge separation and to higher hydrogen evolution. This nanocomposite exhibited H_2 production at a rate of 280 μmol h^{-1} g^{-1}, which was 12.3 and 2.2 times higher than $CaIn_2O_4$ and Fe-TiO_2, respectively. Due to the synthesis method (physical mixing of FTO and CIO), there is no control or uniformity of dispersion of FTO on CIO. In addition, cocatalysts should be deposited on FTO in order to be more effective for hydrogen production. It seems that by applying some coating method the activity of this nanocomposite can improve even more than 280 μmol h^{-1} g^{-1}.

It is worth mentioning that iron oxide is capable of using as metal organic framework (MOF) in diverse morphologies with titanium oxide.[111-113] For instance, Lin's group created a nanocomposite of mixed metal oxide (Fe_2O_3 and TiO_2) via MOF templates.[111] They used MIL-101 MOF (Fe source) to deposit on amorphous TiO_2 and after deposition, they calcined the mixture in order to acquire the nanocomposite of Fe_2O_3/TiO_2. As a result, crystalline octahedral nano-shells were obtained which could produce hydrogen under visible light irradiation. Although TiO_2 can only activate under UV light and Fe_2O_3 has a more positive conduction band than reduction potential of H_2, this novel nanocomposite with a help of Pt metal as a cocatalyst produced 30.0 μmol g^{-1} of hydrogen in 48 hours in the presence of TEA as a sacrificial agent. The reason for this activity is that some iron ions from MIL-101 can be doped into TiO_2 crystallinity during the calcination process and the other converted into Fe_2O_3. Fe_2TiO_5 and Ti-doped Fe_2O_3 are both considered as activated photocatalysts under visible light in H_2 formation because of their small band gaps (Fe_2TiO_5 = 2.2 eV and Ti-doped Fe_2O_3 = 2.1 eV) and their edge of conduction bands which are more negative than reduction potential of H^+.[112] Moreover, further characterizations showed that this material was stable during hydrogen evolution and no decreasing in activity was observed. By introducing this kind of hollow nanostructure, the surface area of the photocatalyst increase significantly that results in higher activity owing to more available active sites. Another example of this type was developed in our group. We proposed a new route to prepare a novel type

of photocatalytic hollow Fe2O3-TiO2 nanostructure using MOF-UMCs as a hard template.[113] In this type of MOF-UMCs materials, each trimeric Fe(III) center possesses terminal water molecules that can be removed by vacuum and temperature treatments to generate Lewis acid sites, to which the amine group of titanium precursor can be grafted via the lone electron pair of nitrogen atom for the preparation of core/titania shell nanostructure, as illustrated in Figure 2.15. This achieved hollow nanostructure of Fe_2O_3–TiO_2–PtO_x photocatalyst possesses two distinct cocatalysts which are deposited separately on two sides of its hollow surface. The distance of two cocatalysts (wall thickness of template) was 15-35 nm that strongly facilitated charge separation and so increased photocatalytic activity. One of the cocatalysts was created from metal clusters of the MOF after calcination, located inside the hollow structure and the other was made from metal doping (PtO_x) on the surface of this nanocomposite. Interestingly, the visible light absorption band edge was extended to 610 nm. Under visible light illumination and in the presence of lactic acid, this nanocomposite could produce 22 μmol h^{-1} hydrogen without any reduction in its activity even after 5 cycles. The total amount of H_2 after five cycles was 110 μmol h^{-1} under visible light irradiation. Although this amount of hydrogen production was not so much in comparison with other photocatalysts, but this approach may be used to develop other hollow structures with higher activity for hydrogen evolution in the visible light region.

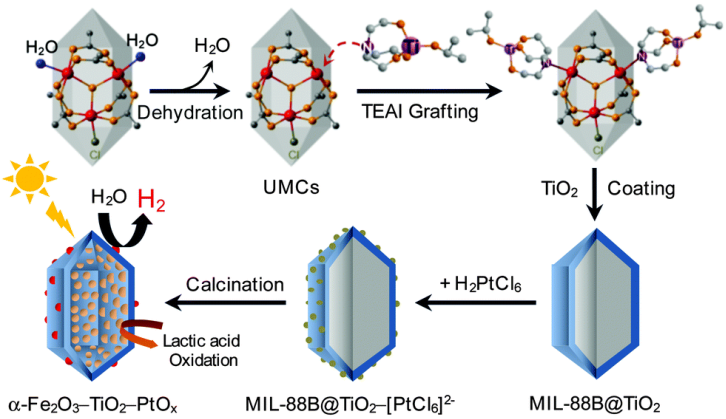

Figure 2.15. Schematic illustration of the formation of the hollow Fe_2O_3–TiO_2–PtO_x nanocomposite.[113]

In addition to metal oxides, scientists tried to mix diverse metal sulfides with titanium oxide due to their higher visible light absorption. CdS is the best metal sulfides to combine with TiO_2 because of its proper conduction band and higher efficiency. Due to the importance of this kind of nanocomposite, different compositions and morphologies will be discussed thoroughly in another

section (Section 2.4). Here, other metal sulfides composites with TiO_2 are explained in detail.[114-118] It was reported that the single nanoparticles of In_2S_3 or Pt/TiO_2 were not active in the H_2 formation under visible light irradiation. However, the combined $In_2S_3/Pt/TiO_2$ nanostructure produced H_2 under visible light at the rate of 135 μmol h^{-1} with the 1% quantum yield at $\lambda \geq 420$ nm.[115] In this nanocomposite, both Pt/TiO_2 and In_2S_3 nanoparticles were in close contact owing to embedding Pt/TiO_2 nanoparticles in the interstices of the In_2S_3. The optimum ratio of $In_2S_3/Pt/TiO_2$ was reported to be 3:2. Furthermore, Jang et al. synthesized a photocatalyst composite of titanium dioxide and $AgGaS_2$ with solid state reaction followed by sol-gel method.[118] In the presence of sulfide and sulfite solution and Pt as a cocatalyst, this composite showed a very good activity for hydrogen under visible light irradiation. Due to the conduction band structure, excited electrons can transfer from $AgGaS_2$ to TiO_2 and from there they can react with protons to produce hydrogen. The maximum quantum yield was 17.5% for the optimum ratio of 1:2 (TiO_2:$AgGaS_2$) and 1% Pt.

Some researchers synthesized nanocomposites of TiO_2 with different carbon based materials such as carbon coated metal, carbon quantum dots, carbon nanotube and graphene.[119-125] For example, Peng's group synthesized a novel nanocomposite of carbon coated Ni (denoted as Ni@C) and TiO_2.[123] This nanocomposite consists of nanorods with 10 nm in diameter and 40-100 nm in length. By using triethanolamine as a sacrificial reagent, this nanostructure could produce hydrogen under visible light irradiation. The highest activity was obtained when 5% of Ni was used in this nanocomposite (300 μmol h^{-1}). Furthermore, the apparent quantum yields are 12% and 7% for $\lambda > 420$ and $\lambda > 520$ nm, respectively. These yields were much higher than for neat Ni@C without TiO_2. Table 2.2 shows some nanocomposites of titanium dioxide as well as their activity under visible light irradiation.

A new ternary nanostructure of three different nanoparticles was synthesized in order to enhance H_2 production under visible light irradiation.[92] Firstly, the authors synthesized nanoparticles of Au with an average size of 40 nm. After this step, they grew TiO_2 nanocrystal as a shell structure on the Au nanoparticles via hydrothermal method according to previous researches.[126] Then, they deposited CdS nanoparticles on the surface of $Au@TiO_2$ core–shell nanostructures. This ternary nanocomposite showed considerable high activity for H_2 evolution rather than both binary

Table 2.2. Different nanocomposites of TiO2 active for hydrogen production (λ>420 nm).

Semiconductor 1	Semiconductor 2	Cocatalyst	Sacrificial reagent	Light Source	Hydrogen production ($\mu mol\ h^{-1}\ g^{-1}$)	Quantum yield (%)	Refs
TiO_2	Carbon coated Ni (Ni@C)	---	Triethanolamine	300 W Xe, $\lambda \geq 420$ nm	2000	12 at λ=420 nm 7 at λ=520 nm	[123]
TiO_2 nanosheet	Graphene	---	Methanol	350 W Xe	736	No data	[119]
TiO_2	In_2S_3	Pt	Na_2S/Na_2SO_3	300 W Xe, $\lambda \geq 420$ nm	1350	1 at λ=420 nm	[115]
TiO_2 mesocrystals	Au nanoparticles	Pt	Propanol	Xe light, λ > 460 nm	0.5	No data	[127]
N,S doped TiO_2	V_2O_5	Pt	Methanol	125 W Hg, $\lambda \geq 400$ nm	2966	No data	[105]
TiO_2	MOF MIL 101	Pt	Triethanolamine	450 W Xe, $\lambda \geq 420$ nm	1250	No data	[111]
TiO_2	MOF MIL 88	PtO_x	Lactic acid	300 W Xe, $\lambda \geq 420$ nm	1100	No data	[128]
TiO_2	$AgIn_5S_8$	Pt	Na_2S/Na_2SO_3	300 W Xe, $\lambda \geq 420$ nm	850	No data	[117]
mesoporous TiO_2	WS_2	Pt	Na_2S	350 W Xe, λ > 430 nm	200	No data	[129]
P25	Carbon quantum dot (CQD)	---	Methanol	500 W Halogen, λ > 450 nm	10	No data	[124]
$AgGaS_2$	TiO_2	Pt	Na_2S/Na_2SO_3	450 W Hg, $\lambda \geq 420$ nm	4200	17.5 at λ=420 nm	[118]
$CaIn_2O_4$	Fe-TiO_2	Pt	KI	300 W Xe, $\lambda \geq 420$ nm	280	No data	[107]
Graphene	Au–TiO_2	---	Methanol	3W LED, λ=420 nm	296	4.1 at λ=420 nm	[120]

nanostructures ($CdS-TiO_2$ or $Au@TiO_2$). This ternary design builds up a transfer path for the photoexcited electrons of CdS to the core Au particles via the TiO_2 nanocrystal bridge and thus effectively suppresses the electron-hole recombination on the CdS photocatalyst. However, this nanocomposite is very complicated to obtain and needs precise synthesis method for each step, which is one of its drawbacks in comparison with other binary nanocomposites for hydrogen production.

2.2.2 Various TiO_2 Phase junction

The most common used phase structures of TiO_2 as photocatalyst are anatase and rutile. Although anatase shows higher activity for hydrogen production in comparison with rutile, P25 Degussa TiO_2 (a mixed-phase of anatase and rutile) exhibits higher photocatalytic activity than pristine anatase or rutile.[130-133]

Zhang et al. synthesized TiO_2 particles with phase junction via calcination of anatase TiO_2. [134, 135] The phase transformation happened on the surface of skin of integrated anatase particles. The TiO_2 with mixed phase on the surface showed higher photocatalytic activity and the activity is closely related to the phase junction formed between two phases. Some researchers investigated the charge transportation between the two phases and found that electrons should move from anatase to rutile because of the higher conduction band edge of anatase compared to rutile.[136-138] Although the potential difference between phase junction of anatase and rutile is very small (~ 0.2 eV), it has been proved to be effective in enhancing hydrogen production from TiO_2.[66, 74]

2.3 Graphitic carbon nitride photocatalysts

Graphitic carbon nitride ($g-C_3N_4$) is a metal-free semiconductor that consists of s-triazine or tri-s-triazine units, as can be seen in Figure 2.16.[139, 140] These units are connected in two-dimensional graphite-like framework by amino groups in each layer and weak van der Waals forces between layers.[141] As a result, this polymeric semiconductor shows very high thermal and chemical stability. It can be synthesized by thermal condensation at high temperature (450-650ºC) form nitrogen-rich compounds such as: cyanamide, dicyanamide, melamine, thiourea and urea (Figure 2.17).[142-147] It should be mentioned that carbon nitride has several phase structures

such as α-C_3N_4, β-C_3N_4, cubic-C_3N_4, etc. with different band gaps. .[148] g-C_3N_4 possesses the lowest band gap of 2.7-2.8 eV among all of other carbon nitride crystal structures, which leads to absorb visible light energy of 450-460 nm.[149]

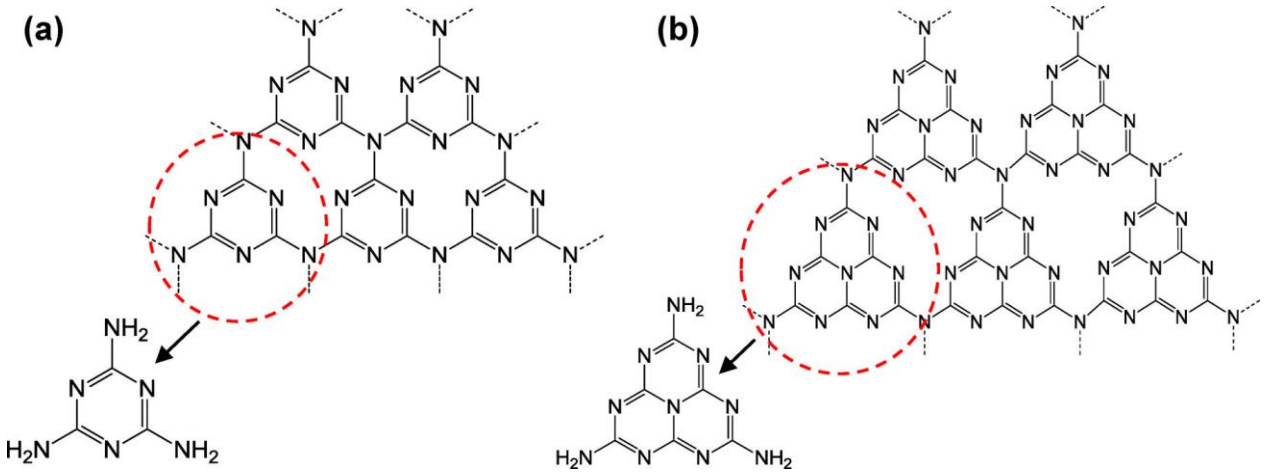

Figure 2.16. (a) Triazine and (b) tri-s-triazine (heptazine) structures of g-C_3N_4.[150]

In 2009, Wang et al. synthesized g-C_3N_4 from cyanamide by pyrolysis at high temperature (400-600 ºC).[151] They showed that this photocatalyst not only produces hydrogen under visible light irradiation from aqueous solution of triethanolamine (TEA), but also it had steady hydrogen production rate over 75 hr. In addition, with a help of TGA and XRD analyses of intermediate compound, they suggested a synthesis procedure, displays in Figure 2.18.[150] Briefly, the cyanamide molecules were converted to dicyandiamide and melamine at the temperature between 200-235 ºC. Simultaneously, ammonia was generated as a by-product of the reaction until all the melamine-based compounds were formed (T~335 ºC). Further increasing in temperature to 390 ºC, rearranged the melamine in order to generate tri-s-triazine units. Finally, between 500-520 ºC polymerization of building units produced g-C_3N_4. It remained perfectly stable until 600 ºC and above that it became unstable and vanished completely above 650 ºC.[150, 152]

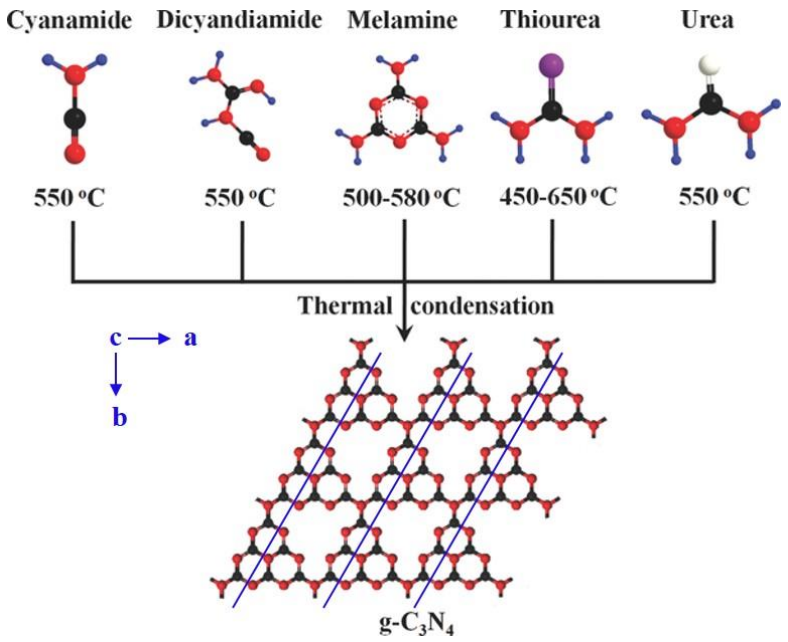

Figure 2.17. Various precursors of g-C_3N_4.[153]

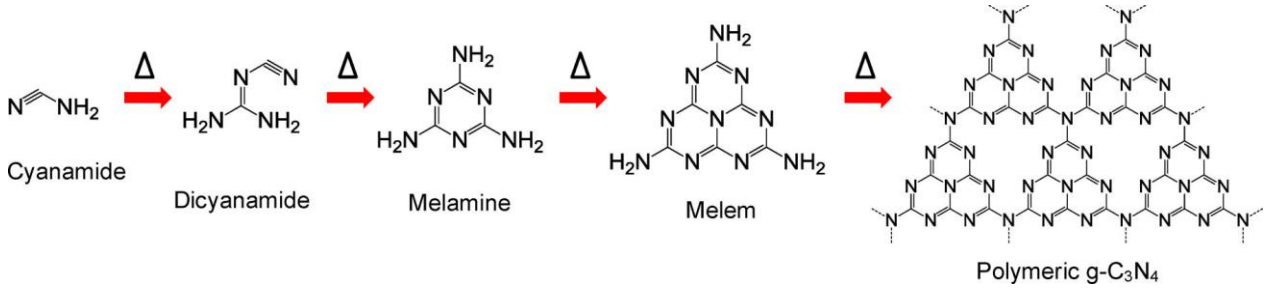

Figure 2.18. Synthesis procedure of g-C3N4 from cyanamide confirmed via TGA and XRD.[150]

Figure 2.19 displays various characterizations of bulk g-C_3N_4 synthesized from cyanamide at 550 ºC. It is clear from UV-visible spectrum that it has a capability of absorbing visible light up to 460 nm. The X-ray diffraction (XRD) curve for analysing the crystal structure of the g-C_3N_4 is shown in Figure 2.19-b. Obviously, it has two distinct peaks at about 13.0º and 27.4º. The former one corresponds to the (100) plane (d=0.681 nm) that is due to the in-plane structural packing motif of g-C_3N_4 (the lattice plane parallel to the c-axis as exhibited by solid line in Figure 2.17). The other peaks can be attributed to interlayer stacking of the long-range aromatic system, which is presented as (002) plane with a d-spacing of 0.326 nm.[154-156] It should be noted that within the

g-C_3N_4 layer, the carbon and nitrogen atoms are connected with covalent bonds, whereas weak van der Waals forces stack its layers together.[157]

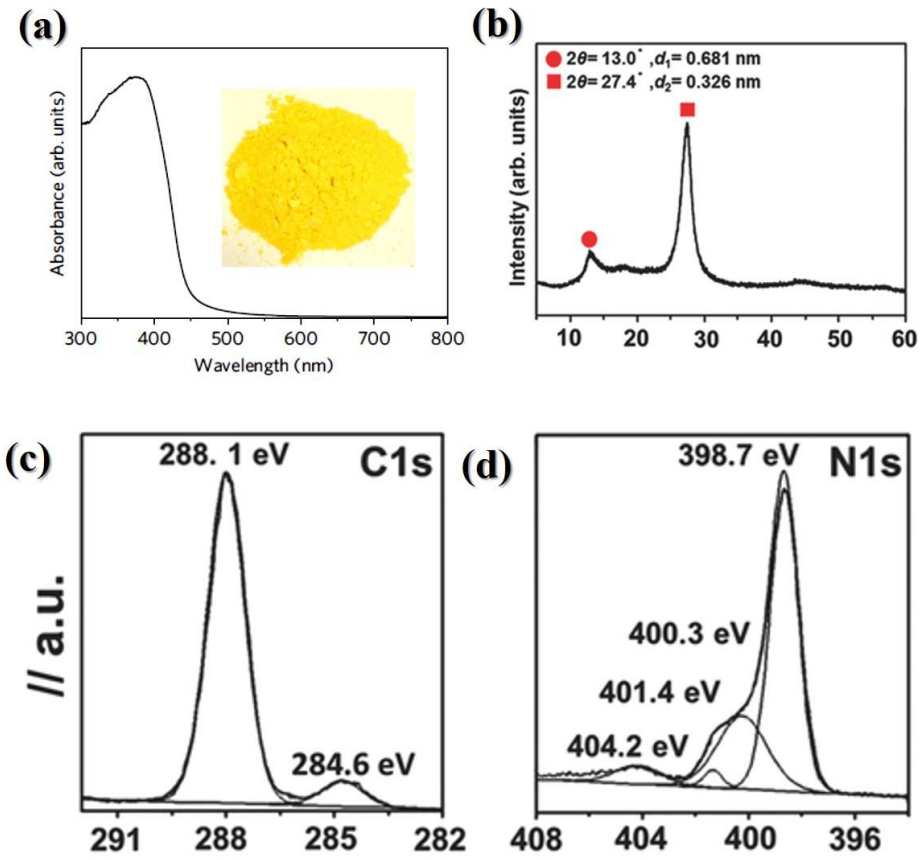

Figure 2.19. a) UV-visible diffuse reflectance spectrum, b) XRD pattern, High-resolution XPS spectra of c) C1s and d) N1s of bulk g-C_3N_4.[151, 153]

The elements status in g-C_3N_4 are examined by X-ray photoelectron spectroscopy (XPS) and are displayed in Figure 2.19-c,d. The C1s curve showed two main peaks at 284.6 and 288.1 eV, that can be related to sp^2-bonded carbon in C−C and N−C=N, respectively. The N1s spectrum can be deconvoluted into four main peaks corresponding to nitrogen status in various bond structures including: the sp^2-bonded in C−N=C (ca. 398.7 eV), tertiary in N− C_3 (ca. 400.3 eV), amino groups with hydrogen atom C−NH (ca. 401.4 eV) and a positive charge localisation in heptazine rings (ca. 404.2 eV). [153, 158, 159] The Bulk g-C_3N_4 has a potential to be one of the best photocatalyst for hydrogen production in visible light region. Nevertheless, it showed very little hydrogen production mainly due to its low specific surface area and high electron-holes recombination process. As a result, many researchers and scientists tried to enhance its hydrogen production by

various methods such as providing large surface area, making nanosheets of g-C_3N_4, utilizing various cocatalysts and creating heterojunctions with other semiconductors.

Due to the structure similarity of carbon bonds in carbon based nanostructures (nanotubes and graphene) with graphite carbon nitride, it is believed that these materials can mix together and as a result photocatalytic efficiency will increase substantially. [145, 147] For instance, g-C_3N_4 nanosheet was mixed with graphene in order to increase visible light photocatalytic activity for H_2 generation.[145] This metal-free nanocomposite could generate hydrogen from an aqueous solution of methanol under light illumination ($\lambda > 400$ nm). By using 1 wt% of graphene with Pt-loaded g-C_3N_4, the H_2 evolution rate was noticeably enhanced from 147 μmol h^{-1} g^{-1} to 451 μmol h^{-1} g^{-1}. Another group tried to modify g-C_3N_4 by introducing carbon nanotubes into its structure.[147] Despite the fact that the new composite and pure g-C_3N_4 are very similar in their properties, the new photocatalyst possessed higher activity (around 2.5 times) than the other one. With optimal amount of carbon nanotubes (2 wt%), it produced 394 μmol h^{-1} g^{-1} hydrogen under visible light illumination because of increasing the lifetime of excited electron and holes and prevent them to recombine together.

Furthermore, other semiconductors can be combined with g-C_3N_4 in order to prevent charge recombination. [143, 144, 160-165] For example, Chai et al. generated a nanocomposite consisting of porous g-C_3N_4 with TiO_2 nanoparticles.[143] According to the close interaction between these nanomaterials, when this nanocomposite was improved by Pt metal as a cocatalyst, it showed hydrogen evolution under visible light illumination ($\lambda > 420$ nm). The maximum hydrogen evolution (178 μmol h^{-1}) was achieved when the mass ratio of g-C_3N_4 and TiO_2 was 70 to 30. Kang et al. synthesized a composite of graphitic carbon nitride and Rh-doped $SrTiO_3$.[144] With help of Pt as a cocatalyst, this photocatalyst could produce hydrogen from aqueous solution of methanol at 410 nm with a quantum yield of 5.5%. Doping Rh into the structure of $SrTiO_3$ provides the donor level in band gap region of $SrTiO_3$:Rh. As a result, the excited holes can easily transfer from $SrTiO_3$:Rh semiconductor to carbon nitride and the excited electrons move from the conduction band of g-C_3N_4 to $SrTiO_3$:Rh. This leads to have high charge separation and higher hydrogen production (2223 μmol h^{-1} g^{-1}) in comparison with each of the semiconductors alone. Table 2.3 shows various heterojunctions of g-C_3N_4 and semiconductors that could improve hydrogen production under visible light.

Another effective method to enhance g-C_3N_4 photoactivity is to increase its specific surface area, which is less than 10 m^2 g^{-1} for the bulk material.[166] Due to its graphite-like layered structure, various methods were suggested to synthesize multilayer and monolayer nanosheets of g-C_3N_4.[154, 167-169] Reducing the thickness of nanosheets causes its band gap to increase due to quantum confinement effect.[154] In thermal exfoliation technique, increasing the time of synthesis up to 4-6 h or recalcining the bulk material again in controlled conditions (low ramping rate, static air or inert gas), led to have nanosheets of g-C_3N_4. As shown in Figure 2.20, the reaction time considerably affects the thickness of g-C_3N_4.[168, 170] Other groups used liquid exfoliation methods to obtain the nanosheets.[154, 169, 171] They usually used a mixture of water and another solvent with appropriate surface energy such as ethanol, isopropanol or dimethyl formamide. Then, ultrasonic bath was used more than 10 hr, in order to transmit require energy for breaking the van der Waals forces between the layers. After this step was completed, a highly uniform and stable suspension of nanosheets of g-C_3N_4 was obtained, as depicted in Figure 2.21. This method was widely utilized for fabricating nanosheets of g-C_3N_4 because of its facile and convenient process.

Some researchers using hard and soft templates in order to produce mesoporous g-C_3N_4 with high specific surface area. For instance, He et al. synthesized mesoporous sucrose-mediated g-C_3N_4 by using thermal condensation of sucrose and melamine.[172] Firstly, they dissolved sucrose in an ethanol aqueous solution, then under continuous stirring, melamine was added. After drying in water bath, the obtained mixture was heated to 600 ºC for 2 hr. During calcination step, oxidation and decomposition of sucrose formed mesoporous g-C_3N_4, as demonstrated in Figure 2.22. As a result, the specific surface area was enhanced to 128 m^2 g^{-1} from 18.6 m^2 g^{-1} of bulk g-C_3N_4.

Table 2.3. Different nanocomposite of graphitic carbon nitride.

Semiconductor 1	Semiconductor 2	Cocatalyst	Sacrificial reagent	Light Source	Hydrogen production ($\mu mol\ h^{-1}\ g^{-1}$)	Quantum yield (%)	Refs
layered g-C_3N_4 sheets	graphitized polyacrylonitrile	Pt	Triethanolamine	150 W Halogen, $\lambda \geq 420$ nm	370	No data	[173]
g-C_3N_4	Nickel sulfide (NiS)	---	Triethanolamine	300 W Xe, $\lambda \geq 420$ nm	447.7	No data	[160]
g-C_3N_4	zinc phthalocyanine	Pt	Ascorbic acid	350 W Xe, $\lambda \geq 420$ nm	12500	1.85 at $\lambda = 700$ nm	[174]
g-C_3N_4	C/N co-doped TiO2	Ag	Methanol	300 W Xe, $\lambda \geq 420$ nm	96	No data	[161]
g-C_3N_4	PEDOT	Pt	Triethanolamine	300 W Xe, $\lambda \geq 420$ nm	327	No data	[146]
g-C_3N_4	WO_3	Pt	Triethanolamine	300 W Xe, $\lambda \geq 420$ nm	110	0.9 at $\lambda = 420$ nm	[162]
g-C_3N_4	carbon nanotubes	Pt	Triethanolamine	350 W Xe, $\lambda \geq 420$nm	394	No data	[147]
g-C_3N_4	$ZnFe_2O_4$	Pt	Triethanolamine	300 W Xe, $\lambda \geq 420$ nm	200.77	No data	[163]
g-C_3N_4	Ag_2S	---	Methanol	300 W Xe, $\lambda \geq 420$ nm	200	No data	[164]

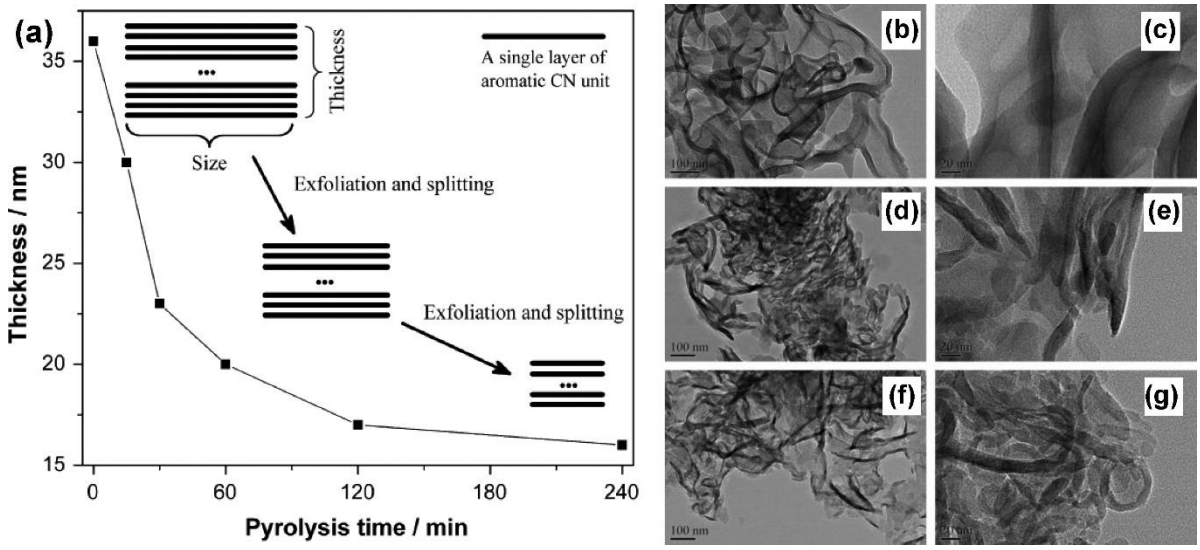

Figure 2.20. (a) Relationship between the pyrolysis duration and layer thickness of g-C_3N_4 and the diagram for the layer-by-layer exfoliation and splitting mechanism of g-C_3N_4 with decreased thickness and size. (b–g) TEM images of g-C_3N_4synthesized at 550 °C for (b–c) 0 min, (d–e) 60 min, and (f–g) 240 min, excluding the heating-up time.[150, 170]

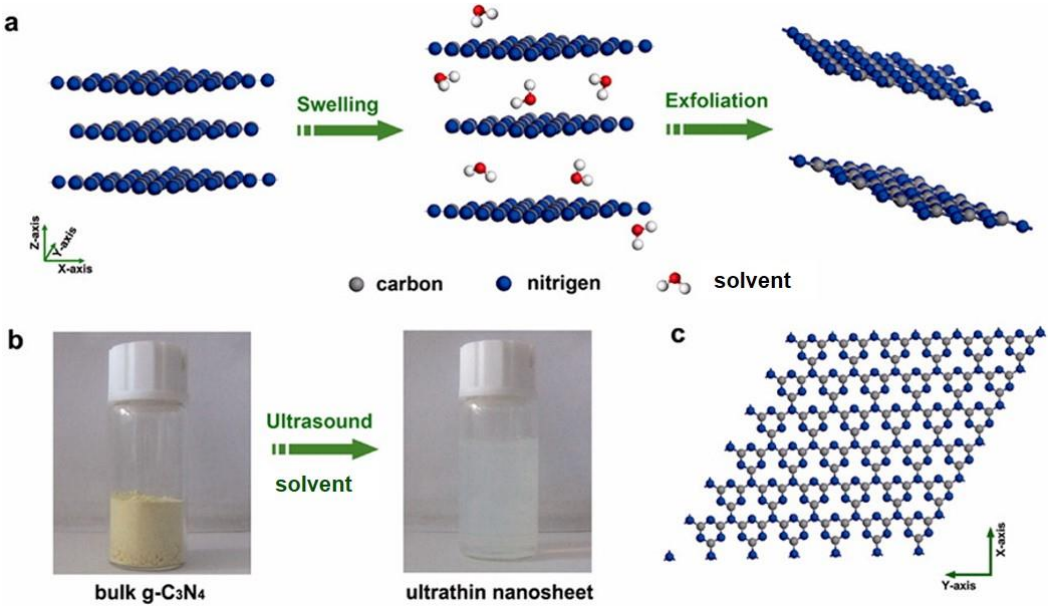

Figure 2.21. (a) Schematic illustration of liquid-exfoliation process from bulk g-C_3N_4 to ultrathin nanosheets. (b) Photograph of bulk g-C_3N_4 and suspension of ultrathin g-C_3N_4 nanosheets. (c) A theoretically perfect crystal structure of the g-C_3N_4 projected along the z-axis.[175]

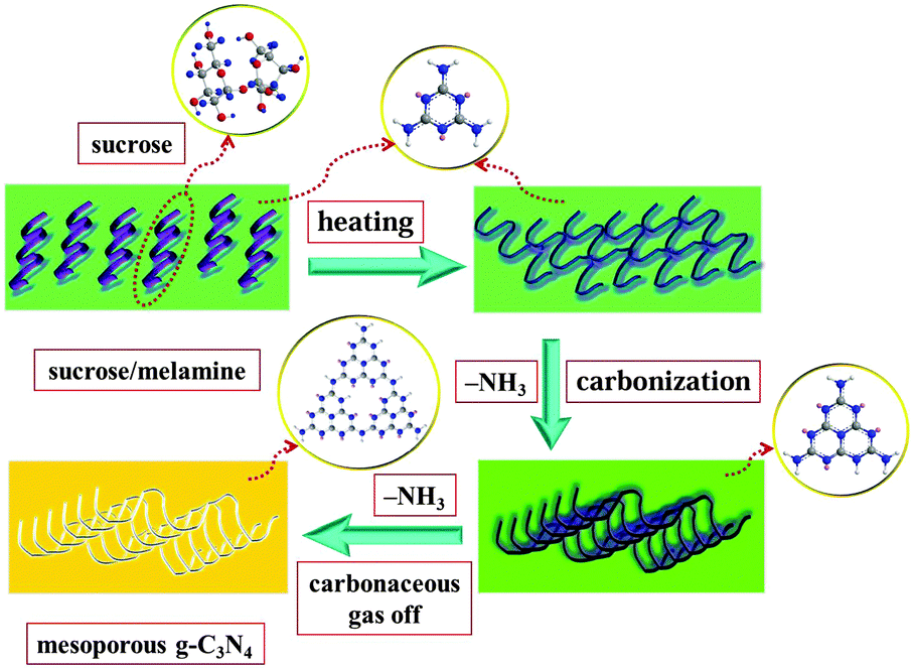

Figure 2.22. Schematic illustration for the formation of mesoporous sucrose-mediated g-C_3N_4.[172]

Another group created honeycomb-like g-C_3N_4 with one-step thermal polymerization of urea in the presence of water at 450 ºC.[176] As illustrated in Figure 2.23, during g-C_3N_4 synthesis procedure, large numbers of soft bubbles from the NH_3 and CO_2 gases were formed, which resulted in having bubble-like structure of g-C_3N_4. Later, these bubbles burst, leaving behind honeycomb nanosheets of g-C_3N_4. This nanostructure not only increases specific surface area, but also helps having multiple light reflections in the porous material as well as increasing reactant diffusion throughout the nanosheets (as demonstrated in Figure 2.23-Right).

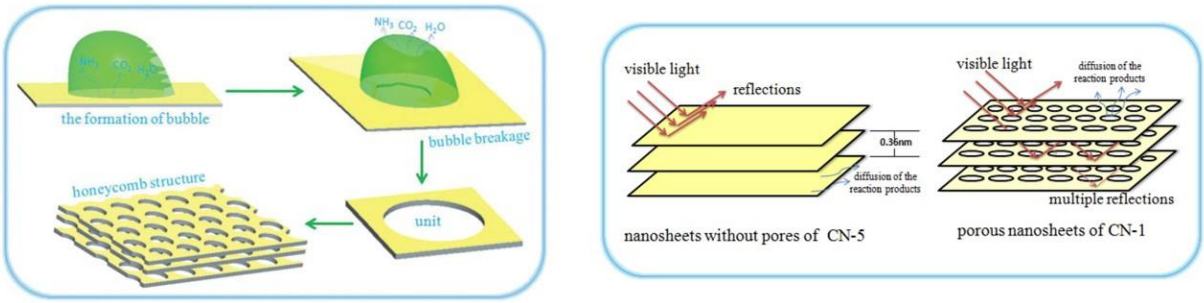

Figure 2.23. (Left) Formation mechanism of the honeycomb-like morphology of g-C_3N_4. (Right) Schematic illustration of the differences between g-C_3N_4 nanosheets with and without pores.[176]

The reaction atmosphere significantly affected the photocatalytic activity of g-C_3N_4 through generating structural defects, carbon and nitrogen vacancies as well as inducing disordered structures. The structural defects are crucial for heterogeneous catalysis because they provide active sites for reactant molecules. In addition, the defects have impacts on electronic band structures and they can introduce additional energy levels between the valence band and the conduction band.[177-179] The defects and lattice disorders can provide band tail states, which are midgap states for excited electron-hole pairs.[180] Thus, the obtained semiconductor can absorb more visible light energy and so it can produce more hydrogen.[181, 182] Furthermore, these defects generate more trapping sites on the surface of semiconductors, which enhance lifetime of excited charges by slowing down the recombination procedure.[183]

Niu et al. synthesized g-C_3N_4 with nitrogen vacancies via modulating the synthesis temperature in static air.[156] These defects left extra electrons in the structure of carbon nitride resulting having nitrogen vancancy-related C^{3+} state in the band gap. Thus, the band gap of the obtained material decreases from 2.74 to 2.66 eV. Nitrogen vacancies can also be obtained by changing the reaction atmosphere to H_2 gas.[184] They observed that H_2 diffusion through the surface to the bulk of g-C_3N_4 in the space originated from the periodic layer stacking along the c-axis of melon (Figure 2.17), can make homogeneous self-modification in layered structure (Figure 2.24)

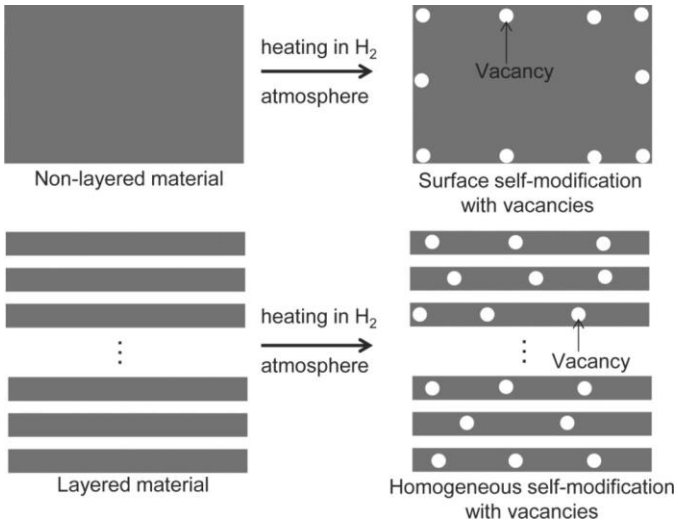

Figure 2.24. Schematic illustration of surface self-modification with vacancies in a nonlayered material and homogeneous self-modification with vacancies in a layered material upon thermal treatment under H_2 environment.[184]

2.4 Zinc cadmium sulfide photocatalyst

Cadmium sulfide (CdS) is one of the best semiconductors for photocatalytic hydrogen production because of its narrow band gap and conduction edge-band position. In other words, it can absorb visible light with long wavelength and also it can reduce protons to hydrogen. However, this photocatalyst has two main disadvantages which are: (1) due to its small band gap, the recombination process of photoexcited electrons and holes is very easy; (2) this semiconductor is unstable under light irradiation and it is effortlessly corroded by excited holes.[185] For these reasons, CdS needs to be combined with other semiconductors in order to overcome its drawbacks.

It has two crystal forms: the hexagonal Wurtzite (found in the mineral Greenokite) and the cubic blend structure (found in the mineral Hawleyite).[186] Although in both forms cadmium and sulfur atoms are in four coordination, the hexagonal crystal structure is more stable than the cubic one.[187] This semiconductor is a n-type 2.42 eV that can be excited via visible light irradiation. It should be noted that its photocatalytic properties and activity are affected by the particle size and the morphology.[185, 188, 189]

Due to a highly visible light absorption of CdS (2.42 eV), scientists tried to enhance photocatalytic efficiencies of CdS with modifying nanostructures of this semiconductor. Nanostructure of CdS provided more active sites for water splitting reaction and so increase its photocatalytic activity.[190] Another technique is preparing CdS in nano-porous structures that can raise the quantum yield up to 60% in the presence of Na_2SO_3 and Na_2S as sacrificial agents ($\lambda \geq 420$ nm).[191] The main reasons for this development in quantum yield are effective charge separation, fast movements of charge carriers, and quick chemical reaction at the interface of CdS nanostructure. Combing CdS nanoparticles with another semiconductor is another way to enhance its photocatalytic efficiency.[192]

Although metal oxides are usually possessing wide band gap and cannot absorb long wavelength of sunlight spectrum, they are very stable during photocatalytic processes. Therefore, some studies were done in order to mix these semiconductors together and obtained more efficient photocatalysts.[59, 193-203] For instance, Wang and co-workers prepared core-shell nanostructures from ZnO and CdS.[193] This nanocomposite was able to split water to produce H_2 with sacrificial reagents. Interestingly, loading RuO_2 cocatalyst showed more activity rather than Pt metal. In addition, the ratio of ZnO to CdS in $(ZnO)_{1-x}(CdS)_x$, strongly affected its photocatalytic

efficiency and it slightly dropped by raising CdS molar ratio. The highest H_2 evolution is 2.96 mmol h^{-1} g^{-1} by x = 0.2, which is 34.4 times and 7.8 times higher than that of ZnO nanorods (prepared by the hydrothermal route) and CdS (prepared by the solid-state route), respectively. As mentioned before, RuO_2 has a great impact on photocatalytic activity resulted in a sudden increase by around 200%. This nanocomposite could constantly produce H_2 for more than 30 h. Hou et al. synthesized a nanocomposite of CdS (2.45 eV) and TaON (2.5 eV) in a core-shell structure.[195] They deposited TaON on the core of CdS and used Pt as a cocatalyst. Due to the band edge positions of these semiconductors, electrons migrate from CdS to TaON and holes can move from TaON to CdS. Although hydrogen evolution rates for pure CdS and TaON were 13.5 and 9 µmol h^{-1}, respectively, this nanocomposite could evolve 306 µmol h^{-1} hydrogen using a sacrificial reagent. Moreover, combining this nanostructure with 1wt% graphene oxide led to produce more than two times higher hydrogens than the previous one with a 31% quantum yield under visible light irradiation. Nonetheless, they didn't examine the stability of this nanocomposite for multiple cycles in longer runtime. Because one of the purpose of combining CdS with other materials is to enhance its stability during reaction time. Usually the photocatalyst should run 3-4 cycles of 3-5 hr of hydrogen production in order to observe its stability under light illumination.

In addition to binary metal oxides, some researchers made a nanocomposite of CdS and ternary metal oxides.[204-207],[110,111] In these nanostructures, generated holes can transfer from CdS to metal oxides, due to their valence band positions, and photoexcited electrons remain in the conduction band of CdS and reduce protons to hydrogen. These charge carriers' movements are completely different than in other nanocomposites. Usually electrons transfer to other semiconductors from CdS but in this case holes transfer and so both charge recombination and photocorrosion are avoided. However, it should be noted that the synthesis procedure of these ternary nanocomposites is usually complicated and needs careful attention in order to obtain desire nanostructure.

Furthermore, CdS can be combined with other metal sulfides in various morphologies such as nanocrystals[208], nanowires[209], nano-layers[210] in order to enhance its efficiency. Among all metal sulfides, ZnS attracts more attention due to its high ability to form solid solution with CdS which results in higher charge separation and more quantum efficiency.[211-218] For example, a solid solution of $(Zn_{0.95}Cu_{0.05})_{1-x}Cd_xS$ was examined with various ratios of Cd for H_2 production

under visible light and in the presence of SO_3^{2-} and S_2^{2-}.[211] This solid solution consisted of nanocrystals of about 2-5 nm and had a band gap of 2.0 eV. This nanostructure showed 508 μmol h^{-1} without any cocatalyst and possesses a quantum yield of 15.7% under visible light when x equal to 0.33. However, by depositing 0.75% Pt, its activity enhanced significantly and hydrogen production and quantum yield reached to 1.09 mmol h^{-1} and 31.8%, respectively. Moreover, this nanocomposite was stable after 3 cycles 12 h. Zhang and al. synthesized a nanocrystal of solid solution ZnS-CdS that was involved in H_2 evolution at 420 nm.[213] They used MoS_2 compound as a cocatalysts and reported that with 0.2 wt% of this cocatalysts, the hydrogen formation was 36 times higher than CdS with noble metals as cocatalysts.[219, 220] Moreover, Liu et al. showed that nano-twin structures of $Cd_{1-x}Zn_xS$ solid solution could produce hydrogen from water without noble metals. Its apparent quantum yield was reported to be 43% at 425 nm in the presence of sacrificial reagents.[214] Another type of nanocomposites of ZnS and CdS is the physical mixture of their nanoparticles without making a solid solution phase. Shen et al. improved nanocrystals of ZnS/CdS (5-10 nm) with In_2S_3 without any surfactant or supports at room temperature and normal pressure.[208] These microspheres could produce hydrogen from aqueous solution of sulfide and sulfite ions with no cocatalysts and it was reported that the quantum yield achieved to 40.9 % at $\lambda \geq 420$nm. The optimum ratio of CdS is 75%, which can produce 8.1 mmol h^{-1} g^{-1} hydrogen. Despite the fact that this nanocomposite showed a very high hydrogen evolution, no detailed observation was done to examine its stability during hydrogen production, which should be considered in further studies.

In addition to solid solution, CdS can mix with other metal sulfides in order to increase hydrogen production under visible light irradiation.[209, 221-223] For instance, TiS_2 and TaS_2 are both semiconductors with small band gap less than 1 eV. A nano-layer combination of one of these two semiconductors with nanoparticles of CdS resulted in high efficient photocatalysts for H_2 evolution from an aqueous solution of benzyl alcohol.[210] The nanocomposite of TiS_2 and CdS could generate 1000 μmol $h^{-1}g^{-1}$ hydrogen, whereas the other one (TaS_2 and CdS) showed 2.3 times higher hydrogen evolution (2320 μmol $h^{-1}g^{-1}$) under visible light irradiation. The reason for this phenomenon was explained by the metallic nature of few-layer TaS_2. In another study, Zhang et al. deposited NiS nanoparticles on the CdS surface with the help of hydrothermal route.[221] They reported that the nanocomposite with 1.2% of NiS had the highest activity and quantum yield. Its quantum efficiency under visible light irradiation ($\lambda > 420$nm) was 51.3 %, which was the highest

photocatalyst activity without noble metal cocatalyst. In addition, its H_2 evolution rate was 2.18 mmol h^{-1} which was 35 times higher than that of alone CdS. Hou et al. decoreated $CdLa_2S_4$ microspheres with CdS nanocrystals by a hydrothermal procedure in order to enhance hydrogen generation.[218] Due to the intimate contact of these nanoparticles and also high dispersion of CdS nanocrystals, this nanocomposite exhibited a significant quantum yield of 54% under visible light region corresponding to 2250 μmol h^{-1} g^{-1}, which was 9 times higher than the pristine $CdLa_2S_4$.

Carbon nanotubes is one of the most famous building block for synthesizing nanostructures that can be combine with diverse semiconductors particularly CdS in order to enhance charge separation step, as demonstrated in Figure 2.25.[224-229] Furthermore, graphene nanosheet has some special properties such as high surface area, high charge carrier mobility (due to its two-dimensional sp^2-hybridized), and good mechanical stability.[230] The intimate contact between CdS and graphene can enhance the migration of photoexcited electrons and surpass the recombination process more efficiently. In principle, photoexcited electrons move from the conduction band of the CdS to graphene and according to great mobility of electrons on the graphene sheets, the recombination process is partially prevented.[227, 229, 231-237] For instance, Li et al. synthesized CdS nanoparticles of about 3 nm in autoclave and they dispersed them on graphene nanosheet completely.[237] This nanocomposite, which had 1 wt% graphene and 0.5 wt% Pt, showed 1.12 mmol h^{-1} hydrogen evolution from a solution of lactic acid. This rate of hydrogen production was around 5 times higher than pristine CdS and the apparent quantum efficiency was reported 22.5% at $\lambda \geq 420$ nm.

There have been different methods to synthesize graphene-based photocatalysts, but the simplest and most direct technique is to mix graphene with target semiconductors.[238-240] The other popular method to provide nanocomposites of various semiconductors with graphene is in situ growth method in which graphene oxide (GO)[195, 237, 241] or reduced graphene oxide (RGO)[242-250] is chosen as starting materials.[251] Nanocrystals of CdS or other semiconductors can grow on the surface of graphene nanosheet via oxygen-containing functional groups which act as nucleation sites.[252] The structure and electrical properties of RGO as well as the location of the conduction band of CdS and RGO lead the photoexcited electrons transfer from CdS to RGO and from there, they can reduce hydrogen atoms (Figure 2.26). Table 2.4 summarized hydrogen

production of different nanocomposite of CdS under visible light irradiation with their quantum yields.

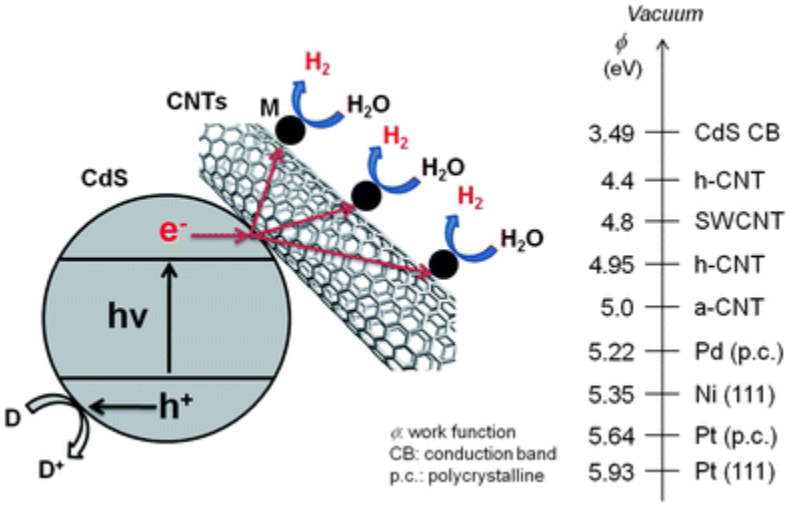

Figure 2.25. Illustration of photocatalytic hydrogen production in CdS/CNT/M suspensions under light irradiation. M and D refer to metal catalyst and electron donor, respectively. On the right-hand side, the reported work functions of selected materials are given. [225]

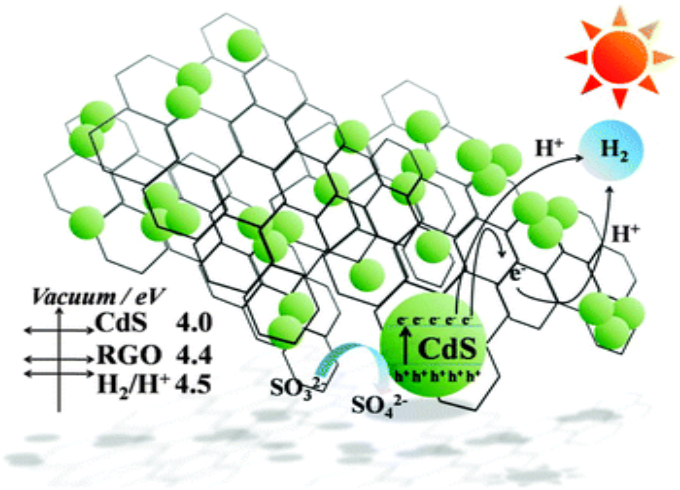

Figure 2.26. Schematic diagram of the proposed mechanism for photocatalytic H_2 production over RGO–CdS.[250]

Table 2.4. Various nanocomposites of CdS active under visible light illumination.

Semiconductor 1	Semiconductor 2	Cocatalyst	Sacrificial reagent	Light Source	Hydrogen production ($\mu mol\ h^{-1}\ g^{-1}$)	Quantum yield (%)	Refs
CdS	SrS	---	Na_2S/Na_2SO_3	300 W Xe, $\lambda > 400$ nm	246	10 at $\lambda = 420$ nm	[209]
CdS	ZnCu	---	Na_2S/Na_2SO_3	300 W Halogen, $\lambda \geq 420$ nm	1693	15.7 at $\lambda =$ 420 nm	[213]
CdS	ZnCu	Pt	Na_2S/Na_2SO_3		3633	31.8 at $\lambda =$ 420 nm	[213]
CdS	CuIn	---	Na_2S/Na_2SO_3	300 W Xe, $\lambda \geq 420$ nm	649.9	2.14 at $\lambda =$ 420 nm	[212]
CdS	CuIn	Pt	Na_2S/Na_2SO_3		2456	26.5 at $\lambda =$ 420 nm	[212]
CdS	ZnO	Pt	Na_2S/Na_2SO_3	300 W Xe	2960	No data	[193]
CdS nanorods	CdSe	Pt	2-propanol	300 W Xe	40500	20 at $\lambda = 450$ nm	[253]
CdS	$Ni/NiO/KNbO_3$	---	Isopropanol	500 W Hg−Xe, $\lambda > 400$ nm	203.5	8.8 at $\lambda >$ 400 nm	[207]
CdS	$Ni/NiO/KNbO_3$	---	Isopropanol	500 W Hg−Xe, $\lambda > 400$ nm	150	4.4 at $\lambda >$ 400 nm	[206]
CdS	$LaMnO_3$	---	Na_2S/Na_2SO_3	300 W Xe, $\lambda \geq 420$ nm	595	No data	[205], [254]
$Cd_{0.8}Zn_{0.2}S$	ZnO	Pt	benzyl alcohol	450 W Xe,	36500	50.4 at $\lambda =$ 400 nm	[217]
CdS nanorods	NiS	---	Na_2S/Na_2SO_3	300 W Xe, $\lambda \geq 420$ nm	1131	6.1 at $\lambda =$ 420 nm	[255]

Table 2.4 Continue.

Semiconductor 1	Semiconductor 2	Cocatalyst	Sacrificial reagent	Light Source	Hydrogen production ($\mu mol\ h^{-1}\ g^{-1}$)	Quantum yield (%)	Refs
$Cd_{0.1}Zn_{0.9}S$	Multi-walled carbon nanotube	---	Na_2S/Na_2SO_3	300 W Xe, $\lambda \geq 420$ nm	1563.2	7.9 at λ = 420 nm	[226]
CdS	CeO_2	---	Na_2S/Na_2SO_3	300 W Xe	223	No data	[197]
CdS	Multi-walled carbon nanotubes	Pt	Na_2S/Na_2SO_3	300 W Halogen, $\lambda > 400$ nm	825	No data	[225]
CdS	MWCNTs	---	Na_2S/Na_2SO_3	300 W Xe, $\lambda \geq 420$nm	4977	2.16 at λ = 420 nm	[224]
CdS	ZnS	Ru	Formic acid	300 W Xe, $\lambda \geq 420$nm	6000	20 at λ = 400 nm	[256]
In_2S_3	CdS-ZnS	---	Na_2S/Na_2SO_3	300 W Xe, $\lambda > 400$nm	8100	40.9 at λ = 420 nm	[208]
$CdLa_2S_4$ microspheres	CdS nanocrystal	Pt	Na_2S/Na_2SO_3	300 W Xe, $\lambda \geq 420$nm	2250	54 at λ = 420 nm	[218]
ZnS	CdS	---	Na_2S/Na_2SO_3	500 W Halogen	46	No data	[216]
TaON	CdS	Pt	Na_2S/Na_2SO_3	300 W Xe, $\lambda \geq 420$nm	1530	15 at λ = 400 nm	[195]
Graphene oxide	CdS@TaON				3165	31 at λ = 420 nm	
ZnO	CdS	---	Na_2S/Na_2SO_3	500 W Xe, $\lambda > 400$nm	851	3 at λ = 420 nm	[198]
$CdOW_4$	CdS	---	Na_2S/Na_2SO_3	500 W Xe	90.25	No data	[204]
reduced graphene oxide	CdS	MoS_2	lactic acid	350 W Xe, $\lambda \geq 420$nm	1980	9.8 at λ = 420 nm	[246]

Table 2.4 Continue.

Semiconductor 1	Semiconductor 2	Cocatalyst	Sacrificial reagent	Light Source	Hydrogen production ($\mu mol\ h^{-1}\ g^{-1}$)	Quantum yield (%)	Refs
nanosized MoS_2/graphene hybrid	CdS	MoS_2	lactic acid	300 W Xe, $\lambda \geq 420nm$	9000	28.1 at λ = 420 nm	[235]
reduced graphene oxide	UiO-66 and CdS	Pt	Na_2S/Na_2SO_3	300 W Xe, λ >400 nm	2100	No data	[245]
vermiculite	CdS quantum dot		Na_2S/Na_2SO_3	300 W Xe, $\lambda \geq 420nm$	920	17.7 at λ = 420 nm	[257]
SiC	CdS particles	Pt	Na_2S/Na_2SO_3	300 W Xe, $\lambda \geq 420nm$	555	0.2 at λ = 420 nm	[258]
framework of structured WO3	orderly depositing Au and CdS	---	Na_2S/Na_2SO_3	300 W Xe, $\lambda \geq 420nm$	1730	No data	[199]
ZSM-5 type metalosilicates	CdS nanoparticles	---	Na_2S/Na_2SO_3	500 W Osram, $\lambda \geq 420nm$	11000	65.62 at λ = 420 nm	[259]
γ-TaON hollow spheres	CdS nanoparticles	MoS_2	Na_2S/Na_2SO_3	300 W Xe, $\lambda \geq 420nm$	3142.5	No data	[200]
ZnO core/shell nanofibers	CdS	---	Na_2S/Na_2SO_3	500 W Xe, $\lambda \geq 420nm$	354	No data	[201]
$ZnIn_2S_4$ heterostructures coupled with graphene	CdS quantum dots	Pt	Na_2S/Na_2SO_3	300 W Xe, $\lambda \geq 420nm$	27000	56 at λ = 420 nm	[236]
Carbon nanotube	$Zn_xCd_{1-x}S$	---	Na_2S/Na_2SO_3	500 W Xe	6030	No data	[227]
Carbon nanotube	CdS	NiS	Na_2S/Na_2SO_3	350 W Xe, $\lambda \geq 420nm$	12130	No data	[228]

Table 2.4. Continue.

Semiconductor 1	Semiconductor 2	Cocatalyst	Sacrificial reagent	Light Source	Hydrogen production ($\mu mol\ h^{-1}\ g^{-1}$)	Quantum yield (%)	Refs
reduced graphene oxide	$Cu_{0.02}In_{0.3}ZnS_{1.47}$	Pt	Na_2S/Na_2SO_3	800 W Xe–Hg, $\lambda \geq 420$ nm	3800	No data	[244]
Ti-MCM-48 mesoporous	CdS	RuO_2	Ethanol	300 W Xe, $\lambda >$ 400nm	2730	36.3 at $\lambda =$ 400 nm	[260]
MoO_3	CdS	---	Na_2S/Na_2SO_3	300 W Xe, $\lambda \geq$ 420nm	5250	28.86 at $\lambda =$ 420 nm	[202]
cubic MCM-48 mesoporous	CdS	Pt	Ethanol	300 W Xe, $\lambda >$ 400nm	1810	16.6 at $\lambda =$ 400 nm	[261]
Reduced graphene oxide Ga_2O_3	CdS quantum dots	---	Na_2S/Na_2SO_3 Lactic acid	300 W Xe, $\lambda \geq$ 420nm 300 W Xe, $\lambda \geq$ 420nm	4200	10.4 at $\lambda =$ 420 nm	[243]
Reduced graphene oxide Ga_2O_3	CdS quantum dots	Pt	Na_2S/Na_2SO_3 Lactic acid		9052	43.6 at $\lambda =$ 460 nm	[203]
In_2O_3 TiS2	CdS	---	Benzyl alcohol	450 W Xe, $\lambda >$ 400nm	9382	45.3 at $\lambda =$ 460 nm	[210]

Table 2.4. Continue.

Semiconductor 1	Semiconductor 2	Cocatalyst	Sacrificial reagent	Light Source	Hydrogen production ($\mu mol\ h^{-1}\ g^{-1}$)	Quantum yield (%)	Refs
MCM-41	CdS	---	Triethanolamine	300 W Xe, $\lambda \geq$ 430nm	47.1	No data	[262]
$AgGaS_2$	CdS	Pt	Na_2S/Na_2SO_3	450 W Hg, $\lambda \geq$ 420 nm	4730	19.7at λ = 420 nm	[263]
reduced graphene oxide	CdS	$Ni(OH)_2$	Na_2S/Na_2SO_3	300 W Xe, $\lambda \geq$ 420nm	4731	No data	[242]
graphene oxide	CdS	---	Na_2S/Na_2SO_3	300 W Xe, $\lambda \geq$ 420nm	3410	4.8at λ = 420 nm	[241]
graphene oxide	CdS clusters	Pt	lactic acid	350 W Xe, $\lambda \geq$ 420nm	5600	22.5at λ = 420 nm	[237]
N-graphene	CdS	---	Na_2S/Na_2SO_3	300 W Xe, $\lambda \geq$ 420nm	1050	No data	[234]
g-C_3N_4	CdS quantum dots	Pt	Methanol	300 W Xe, $\lambda \geq$ 420nm	348	No data	[264]

Zinc sulfide (ZnS) is a semiconductor with a direct band gap of 3.12-3.70 eV that can be found in nature as the mineral sphalerite[265, 266] Generally, Zn and S atoms are located in tetrahedral coordination in order to create two crystal structures for ZnS. The more stable cubic form is known as sphalerite or zinc blende and another one has hexagonal structure and is called as mineral Wurtzite.[187] It is evident that this semiconductor cannot generate hydrogen under visible light illumination due to its large band gap.

Recently, a group of researchers created a nanocomposite of ZnO/CdS in a core/shell structure.[267] They used a simple solvothermal method to synthesized CdS nanorods after a shell of ZnO was deposited on their surface via a solution deposition technique. They observed that it showed a very high activity for hydrogen evolution under visible light irradiation and they reported to obtain 44% quantum yield at 420nm. The reasons to have such a high photocatalytic activity are as follow: (1) the transparency of ZnO thin shell allowed CdS to absorb all visible light energy; (2) the photoexcited electrons can transfer to ZnO conduction band from CdS because of the favorable energy band structure; (3) the in-situ ZnS formation prevents CdS from photocorrosion process and also enhances charge separation.

Jiang et al. created a core shell nanocomposite of ZnS and CdS, in which CdS nanorods are decorated by ZnS nanoparticles.[268] As a result, an intimate contact was formed between two semiconductors, which led the electronic structures to be coupled together. Thus, the photogenerated charge carriers could easily move between them which caused an improvement in both hydrogen evolution and photostability of the synthesized nanocomposite. The apparent quantum efficiency was reported to be around 17% at 420 nm.

It is proved that a solid solution of ZnS and CdS not only can produce hydrogen in the visible light region, but also it resolves the photocorrosion issue of CdS.[269-271] Therefore, considerable efforts have been done to synthesize zinc cadmium sulfide ($Zn_xCd_{1-x}S$) solid solution in various sizes (bulk and nanoscale), morphologies, and crystal structures. Interestingly, most of them were successful and could generate hydrogen under visible light with high quantum efficiencies.

Dai et al. deposited CoP semiconductor as a cocatalyst on the surface of $Zn_{0.5}Cd_{0.5}S$ nanorods with two-step in-situ chemical deposition.[272] The nanoparticles of CoP are uniformly deposited on the surface of the solid solution and made intimate contact with nanorods, as demonstrated in Figure 2.27. Obviously, the excited electrons transfer from $Zn_{0.5}Cd_{0.5}S$ to conduction band of CoP and there they react with protons. The CoP not only provides active sites and plays as a cocatalyst in this configuration, but also it increases charge separation process due to its lower conduction band edge than $Zn_{0.5}Cd_{0.5}S$. As a result, with the optimum amount of CoP (5%) this heterojunction generated 20 times more hydrogen compared with pure $Zn_{0.5}Cd_{0.5}S$. Interestingly, this noble-metal-free cocatalyst could produce more than twice hydrogen as Pt-loaded $Zn_{0.5}Cd_{0.5}S$. Another group deposited novel AuPd bimetallic as cocatalyst on the surface of $Cd_{0.5}Zn_{0.5}S$ by an in-situ chemical

deposition technique.[273] It produced 12 times higher hydrogen than pure $Cd_{0.5}Zn_{0.5}S$ due to its significant photogenerated charge separation efficiency.

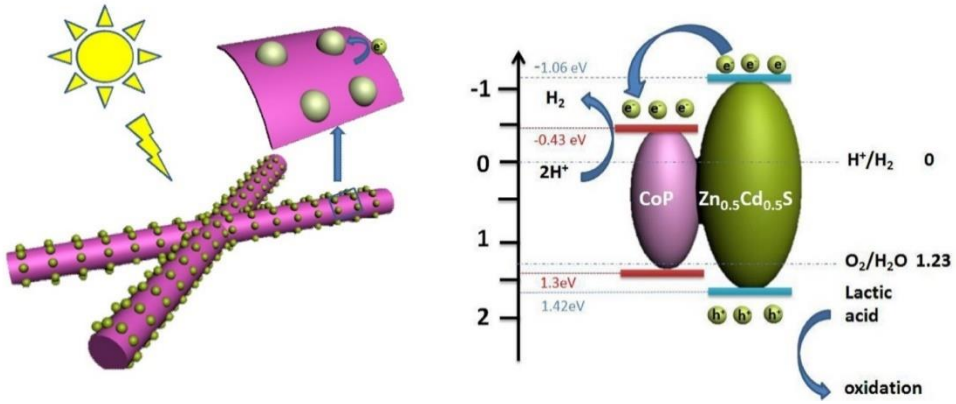

Figure 2.27. Schematic illustration for the charge transfer and separation in $CoP/Zn_{0.5}Cd_{0.5}S$ system and proposed mechanism for photocatalytic H_2 production under visible light irradiation.[272]

Another group synthesized a solid solution of $Zn_xCd_{1-x}S$ by solvothermal methods using ethylenediamine as the solvent and thioacetamide as the source of sulfur.[269] They obtained homogeneous solid solution of $Zn_xCd_{1-x}S$ ($0.3 \leq x \leq 0.5$) in the forms of nanorods and nanoparticles. Interestingly, $Zn_{0.5}Cd_{0.5}S$ exhibited an excellent hydrogen production without using any kind of cocatalyst. It generated hydrogen under visible light irradiation at a rate of 1097 μmol h^{-1} ($\lambda \geq 420$ nm) corresponding to the quantum efficiency of 30% at 420 nm. Nevertheless, the stability of this photocatalyst declined over time and over various cycles because of the Zn^{2+} leaching process during photocatalytic reaction which reduced its crystallinity and generated some lattice defects in the structure of the solid solution.

2.5 Other nanocomposites photocatalysts

In spite of above nanocomposites and nanostructures, scientists have tried to synthesize and combined other nanoscale semiconductors in order to achieve high efficient photocatalysts for hydrogen evolution under visible light illumination. 1D and 2D nanoparticles and nanostructures such as nanowires, nanotubes, nanorods, nanobelts, nanosheets, and nanoflates, have been interested among researchers in the last decade for water splitting via sunlight.[274-287] The combination of these kinds of nanostructures can enhance charge separation effectively and prevent the recombination process and so increase photocatalyst efficiency as summarized in Table 2.5.

Andrew Frame et al. found that CdSe nanoribbons were active in photocatalytic H_2 evolution from S^{2-}/SO_3^{2-} solution under visible light, whereas bulk CdSe was not.[282] By linking these nanoparticles with MoS_2 nanoplates, they activity enhanced about four times and so their quantum yields reached to 9.2% at 440 nm. Interestingly, in this nanocomposite Pt cannot be used as a cocatalyst due to sulfide poisoning of surface sites.

Jing et al. synthesized Cu-doped core/shell tubular nanocomposite of ZnO/ZnS.[283] They tried to deposit Cu-doped ZnS nanoparticles on the outside of ZnO nanotubes. As a result, this nanocomposite showed higher hydrogen evolution than undoped ZnO/ZnS nanocomposite. Copper ions act as donor level to induce visible light response of ZnS and thus excited electrons can migrate from ZnS to ZnO and from there they reduce protons.

Two ferrites chemical of calcium (CFO) and magnesium (MFO), i.e. $CaFe_2O_4$ and $MgFe_2O_4$ were used to synthesize nanocomposites for H_2 evolution reaction.[285] Due to the difference band position of these semiconductors, photoexcited electrons transfer from $CaFe_2O_4$ to $MgFe_2O_4$, whereas the holes can move vice versa. Both of CFO and MFO are active for hydrogen production under visible light irradiation when promoting with cocatalysts (Pt and RuO_2 for CFO and MFO, respectively). However, the nanocomposite of CFO and MFO produced 82.8 mmol h^{-1} g^{-1} with quantum yield of 10.1% which was an order of magnitude higher than RuO_2/MFO or Pt/CFO.

Pradhan et al. synthesized mesoporous nanocomposite of Fe/Al_2O_3–MCM-41 with size of 50 nm. They reported that this photocatalysts with 5 wt% of Fe had the hydrogen production activity under visible light (146 µmol h^{-1}) with the quantum yield of 6.1%. The main reason for such activity is due to the properties of mesoporous materials which are high pore volume, narrow pore size distribution and high surface area. Furthermore, iron doping on the surface helped to absorb visible light, although the mesoporous nanocomposite by itself didn't show any activity for $\lambda > 400$ nm.[286]

Table 2.5. Other nanocomposites for hydrogen production under visible light irradiation.

Semiconductor 1	Semiconductor 2	Cocatalyst	Sacrificial reagent	Light Source	Hydrogen production ($\mu mol\ h^{-1}\ g^{-1}$)	Quantum yield (%)	Refs
ZnS	ZnO core/shell nanotube	Pt	Na_2S/Na_2SO_3	300 W Xe, $\lambda \geq 420nm$	18	No data	[283]
$NaNbO_3$ nanorods	In_2O_3 nanoparticles	Pt	Methanol	300 W Xe, $\lambda \geq 420nm$	16.4	1.45 at λ = 420 nm	[284]
$MgFe_2O_4$	$CaFe_2O_4$	RuO2 on guest and Pt on host	Methanol	450 W W-Arc, $\lambda \geq 420$ nm	82.1	10.1 at λ = 420 nm	[285]
Al_2O_3–MCM-41	Fe	---	Methanol	150 W Hg, $\lambda \geq 400nm$	1460	6.1 at λ = 400 nm	[286]
Fe_2O_3	Fe_4N	---	---	300 W Xe, $\lambda \geq 420nm$	25	1.7 at λ = 400 nm	[287]
WO_3	Au	Pt	Glycerol	300 W Xe, $\lambda \geq 420nm$	132	0.2 at λ = 420 nm	[288]
Ta_2O_5	Au	Pt	Methanol	350 W Xe, $\lambda \geq 420nm$	55	No data	[289]
ZnS–Bi_2S_3 nanorods	ZnO	---	Glycerol	300 W Xe, $\lambda \geq 420nm$	310	No data	[290]
Rh-doped $SrTiO_3$	$BiVO_4$	Ru	---	350 W Xe, $\lambda \geq 420$ nm	200	1.6 at λ = 400 nm	[291]
ZnO	In_2O_3	---	Methanol	300 W Xe, $\lambda \geq 420$ nm	1784	No data	[292]
$SrTiO_3$ (La,Cr)	Sr_2TiO_4	Pt	Methanol	300 W Xe, $\lambda \geq 420$ nm	24	No data	[293]
Bi–$NaTaO_3$	Bi_2O_3	---	Methanol	300 W Xe, $\lambda \geq 420$ nm	102.5	No data	[294]
$GdCrO_3$	$Gd_2Ti_2O_7$	---	Methanol	350 W Hg, $\lambda \geq 400$ nm	1231.5	4.1 at λ = 400 nm	[295]

Table 2.5. Continue.

Semiconductor 1	Semiconductor 2	Cocatalyst	Sacrificial reagent	Light Source	Hydrogen production ($\mu mol\ h^{-1}\ g^{-1}$)	Quantum yield (%)	Refs
$Ag_3PW_{12}O_{40}$	Carbon quantum dots	Ag	---	300 W Xe, $\lambda \geq 420$ nm	3.8	4.9 at $\lambda = 480$ nm	[296]
$Cu_{1.8}S$	ZnS	---	Na_2S/Na_2SO_3	300 W Xe, $\lambda \geq 420$ nm	467	No data	[297]
2D ultrathin curled $ZnIn_2S_4$ nanosheet	MoS_2	---	Na_2S/Na_2SO_3	300 W Xe, $\lambda \geq 420$ nm	975	No data	[298]
In_2O_3	$Gd_2Ti_2O_7$	---	Methanol	300 W Xe, $\lambda \geq 420$ nm	5789	No data	[299]
$K_2La_2Ti_3O_{10}$	$ZnIn_2S_4$	---	Na_2S/Na_2SO_3	300 W Xe, $\lambda \geq 420$ nm	2096	No data	[300]
Ta_2O_5	In_2O_3	Pt	Methanol	300 W Xe, $\lambda \geq 420$ nm	10	No data	[301]

2.6 Conclusion and future developments

In this chapter, firstly we presented an introduction about the fundamentals of photocatalysis process and how it can be used to generate hydrogen from solar energy and water. After that, the overall water splitting procedure and using sacrificial chemicals to facilitate this process for hydrogen production was discussed completely. In addition, we talked about how the photocatalytic activity of a photocatalyst was calculated via the quantum efficiency formula (Equation 2.7). Then, a brief introduction about cocatalysts, helped us to understand their important roles in photocatalysis application specially in hydrogen evolution form water splitting. Moreover, a discussion about various configurations of heterojunctions in semiconductors based on their conduction and valence bands positions were presented completely.

TiO_2 as the first and the most well-known photocatalyst was discussed thoroughly and its challenge to evolve hydrogen in visible light region was mentioned. Then, we talked about various nanocomposites structures between TiO_2 and other visible light active photocatalysts. In addition, the improvement in hydrogen production before and after applying heterojunctions was discussed together. The heterojunctions mostly increased hydrogen evolution due to enhancement of charge separation process. In other words, one kind of photogenerated charge carriers (electrons) migrate from one semiconductor to another, and from there they reduced protons. However, the other photoexcited charge carriers (holes) stayed in the first photocatalyst. Therefore, charge recombination process declined significantly and so hydrogen generation was improved.

After that, graphitic carbon nitride (g-C_3N_4) and its physical and chemical properties were completely explained. Furthermore, its potentials such as a narrow band gap and challenges such as low specific surface area and high rate of charge recombination, to generate large amount of hydrogen were discussed. Then, different approaches to improve its photocatalytic activity were reviewed. They are including creating heterojunctions with other semiconductors, using templates to increase its specific surface area, synthesizing nanosheets of g-C_3N_4 and generating elements vacancies such as carbon vacancies throughout the nanosheets. Although most of the methods displayed significant improvement in hydrogen generation, more works need to be done owing to g-C_3N_4 special physical and chemical characteristics.

Finally, the zinc cadmium sulfide ($Zn_xCd_{1-x}S$) photocatalyst was introduced and its features as a solid solution of two semiconductors (ZnS and CdS) were discussed. As a result, a solid solution of $Zn_xCd_{1-x}S$ possesses a controllable narrow band gap (via ratio of Zn/Cd) as well as high stability to produce hydrogen under visible light illumination. Its crystal morphologies between hexagonal and cubic, affected directly on its activity. Moreover, creating some defects in its structure helped to have more active sites for reducing protons. Even though this photocatalyst showed a good hydrogen production without any cocatalysts, many works were investigated the application of noble metals as well as noble-metal-free cocatalysts on its hydrogen production. They observed that utilizing cocatalysts enhanced its photocatalytic activity considerably and so more researches require for investigate this photocatalyst with other cocatalysts.